Characterization of injection molded HDPE using SAXS and WAXS

Determination of the HDPE structure for post-mortem and in-situ mechanical deformation

Master's thesis in Master of Physics

Linnea Rensmo

DEPARTMENT OF PHYSICS

CHALMERS UNIVERSITY OF TECHNOLOGY
Gothenburg, Sweden 2022
www.chalmers.se

Master's thesis 2022

Characterization of injection molded HPDE using SAXS and WAXS

Determination of the HDPE structure for post-mortem and in-situ mechanical deformation

LINNEA RENSMO

CHALMERS
UNIVERSITY OF TECHNOLOGY

Department of Physics
Division of Materials Physics
Chalmers University of Technology
Gothenburg, Sweden 2022

Characterization of injection molded HDPE using SAXS and WAXS
Determination of the HDPE structure for post-mortem and in-situ mechanical deformation
LINNEA RENSMO

Supervisors: Linnea Björn, Department of Physics,
Chalmers University of Technology
Elin Persson Jutemar, Tetra Pak®
Examiner: Marianne Liebi, Department of Physics,
Chalmers University of Technology

Master's Thesis 2022
Department of Physics
Division of Materials Physics
Chalmers University of Technology
SE-412 96 Gothenburg
Telephone +46 31 772 1000

Typeset in LaTeX
Printed by Chalmers Reproservice
Gothenburg, Sweden 2022

Characterization of injection molded HDPE using SAXS and WAXS
LINNEA RENSMO
Department of Physics
Chalmers University of Technology

Abstract

Plastic materials are used in many of our every day commodities. Its structure may vary depending on which material it consists of and the applied process conditions. The present work was carried out to contribute to the knowledge of the material structure of a certain plastic material called high-density polyethylene, or HDPE, produced through a manufacturing process called injection molding. The project was carried out in collaboration with Tetra Pak® that uses HDPE as a component in their packages.

The aim of the thesis was to characterize the structure of the material HDPE during mechanical deformation. When the material is being produced the shearing forces within the material in injection molding leads to a distribution of different microstructures through the thickness of the material. The structures of the material's full thickness as well as the different layers, that were formed during molding, were investigated. The structure of undeformed HDPE is relatively well-know, and this work investigated how the structure changed after the material was subject to a mechanical deformation. To get deeper insight into such changes, the material was furthermore investigated with in-situ testing, of structural changes during mechanical deformation.

The experimental characterization was performed by means of Small- and Wide-Angle X-ray scattering (SAXS and WAXS) using both laboratory X-ray sources and synchrotron X-ray sources. The scattering experiments showed different microstructures of HDPE on different length-scales. The structures on different length-scales could be distinguished before and after the material had been deformed. During the uniaxial in-situ tensile tests, the deformation sequence of the structures could be monitored, and give an explanation of material behavior under mechanical stress. This information contributes to the general understanding of deformation of plastic materials.

Keywords: HDPE, Scanning SAXS/WAXS, in-situ SAXS WAXS, injection molded polyethylene

Acknowledgements

This work was carried out at the Materials Physics division, Chalmers in cooperation with Tetra Pak Packaging Solutions® in Lund. I would like to thank my examiner Marianne Liebi for giving me the opportunity to do this interesting project and giving me great possibilities to learn, not only the theory of the thesis, but how it is to work in a scientific environment.

I would like to thank my supervisors Elin Persson Jutemar, at Tetra Pak® , and Linnea Björn at Chalmers for all the help throughout the project. The extensive knowledge of the field that Elin posesses has helped me a lot throughout the project. There were no questions from the project that Elin could not find an explanation to. A huge thanks to my supervisor Linnea for tirelessly scribbling explanations on her post-its, again and again, until everything was clear. There would not be a master thesis without your patience.

I would furthermore like to thank Jonathan Avaro, scientist at Empa in Switzerland, for helping me with the in-situ tensile experiments. Thank you for sharing your time and effort to help me make the experiments work so well, against all odds.

I would also like to thank the research group that I have collaborated with for being so inviting. Thanks to Eskil Andreasson and Fredrik Ottenklev at Tetra Pak for the valuable input. Thanks to the scientists at PSI for helping me with the synchrotron measurements; Christian Appel and Ana Diaz, as well as Marianne Liebi and Jonathan Avaro again. I am furthermore grateful for the financial support from FibRe.

Linnea Rensmo, Gothenburg, June 2022

Contents

List of Figures

List of Tables

List of Acronyms

Below is the list of acronyms that have been used throughout this thesis listed in alphabetical order:

CD	Cross Direction
HDPE	High Density Polyethylene
MD	Machine Direction
PSI	Paul Scherrer Institute
SAXS	Small Angle X-ray Scattering
SLS	Swiss Light Source
WAXS	Wide Angle X-ray Scattering

1
Introduction

Polymers are as old as life on earth [1]. Since then, both synthetic and natural polymers have been a key building block of humans as well as the world around us. They are macromolecules consisting of numerous repeating subunits and are a component of many systems, from biological DNA and protein to manufactured silicone and plastic. Since the early days of human craftsmanship, we have utilized polymers for everyday commodities. Materials were composed of polymers in the form of linen for clothes as well as cellulose for paper. Since 1907, when the first synthetic polymer in the form of bakelite was invented, the polymer science field has opened up for a whole new world of possible materials and applications [2].

Plastics are made of organic polymers, commonly from oil or petroleum, and is a subdiscipline of polymer science. Polymers can materialize naturally, but plastics are solely man-made. Some plastic materials have the beneficial physical property of being moldable and versatile with high elasticity, which opened up for endless possibilities when they were first discovered. Plastics are currently used everywhere around us, for example in textiles, construction and consumer products [3].

Tetra Pak®, a multinational food packaging and processing company, frequently uses plastic for their packaging solutions. The famous tetrahedron shaped container was their first product and since then the development of different shapes and materials for food containers has substantially facilitated safe food storage and distribution. The number of different packages has rapidly increased. Originally, they were made only from carton laminate but later included plastics in the form of caps and sturdy packaging tops. Tetra Pak® performs plenty of research in understanding and developing their materials [4].

Lately, efforts have been made to find a material with comparable properties to current plastic materials, however with a smaller environmental impact throughout the product's life cycle. Most plastic materials today are made from oil, which is a non-renewable resource and only 8% of the produced plastic in Sweden in 2017 was recycled to new plastic material [5]. Attempts to produce plastics made from biomaterials in a large scale are not yet sufficiently efficient [6].

One way of finding materials with the same properties as plastic could be to understand the structure of the material on a small scale and furthermore tailor biobased materials from that model. Insights into the structural properties of plastics are therefore important, as well as connecting the structure to the mechanical prop-

erties. The long polymer chains in plastics can arrange in both crystalline and amorphous regions in varying amount and therefore allow for different features of the material. Furthermore, to produce plastic with the right amount of plasticity and durability for food packaging it is vital to understand the structure and its attributes.

The outlook of this thesis is to contribute to the understanding of polymer structures. More precisely a plastic called high density polyethylene, or HDPE, will be investigated. HDPE is the material commonly used in Tetra Pak's® packaging solutions. To shape the investigated material, a process called injection molding is used. Both HDPE and injection molding are presented in detail later in this work. By themselves, they are widely understood, but as a conjunction more is to be discovered. This work focuses on characterizing the structure of HDPE produced by injection molding and how structures develop due to external forces, which is significant for further development of the material. Tetra Pak® can furthermore use the characterization to build computational models of polymeric materials, which will help them make the production of new materials more efficient.

1.1 Aim

The aim of this thesis is to investigate the structure of HDPE produced using injection molding. The methods used will mainly be Small- and Wide-Angle X-ray Scattering, also called SAXS and WAXS, which are presented more in detail in section 2. The aim is to examine the structure before, during and after tensile testing, a technique used to deform the plastic by applying a pulling force, and see how the structures change during deformation. During injection molding the sample forms layers of different structures, the difference in structure between these layers will be investigated.

1.2 Limitations

The material HDPE will be the focus of this work; no other polymers will be included and there will be no comparison between different materials. Only some specific properties of the material will be investigated, for example the structure and sizes of the crystalline and amorphous layers. Tensile testing will take place, but no further strength or toughness tests. The methods used will be SAXS and WAXS since these methods have a resolution on the wanted scales (as described in the Theory section). There are more characterization techniques for polymers, but only the methods mentioned will be used for this work.

1.3 Previous Research

In the almost 100 years that the plastic material HDPE has been produced there has been a lot of research of the material. Already in the 1960's the undeformed structure was investigated and mapped. Since then, the research has developed to include analysis of the structure during deformation, annealing and compression et cetera. The number of articles published regarding HDPE shows the considerable impact of such a widely used plastic as well as the versatility of the material [7]. The structures of HDPE, however, vary considerably depending on how it is manufactured and stretched. None of the previous work specifically explains of how the structure of injection molded HDPE during in-situ deformation changes.

2
Theory

The theory section includes a description of the two major interests of the work, namely the method of scattering and the polymer material.

2.1 Small- and Wide-Angle Scattering

The method used in this work is Small- and Wide-Angle Scattering (SAXS and WAXS) which builds on the principle of scattering of photons from repeating substructures of a material [8]. To explain the working principle of SAXS and WAXS, theory of crystal structure as well as scattering is needed and will be presented next.

2.1.1 Crystalline and Amorphous Structures

Solid state materials can be divided into crystalline and amorphous substances, identified by the ordering of the structure. Long-range order means that the same structure can be found in the material, no matter position. In crystalline samples this ordering is described by the unit cell, which is the smallest portion of a crystal lattice that represents the three-dimensional pattern of the entire crystal, as shown in Figure 2.1. Since the unit cell is repetitive, the whole crystal can be described with a proper description of the unit cell, often described by a crystal lattice and a lattice parameter [9]. The crystal lattice describes the arrangement of atoms in the unit cell while the lattice parameter describes the dimensions of the unit cell.

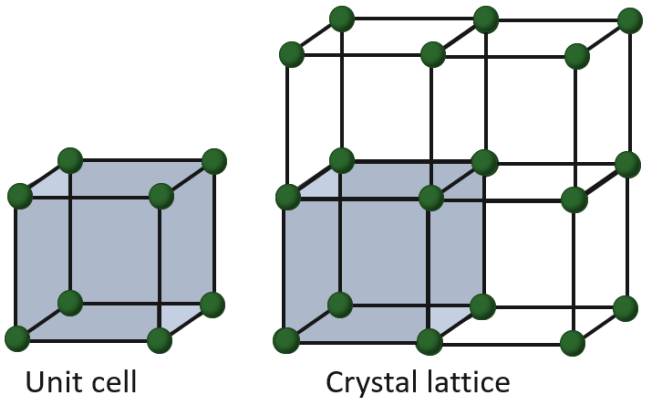

Figure 2.1: A unit cell of a simple cubic structure to the left, the crystal lattice built from repeating units of the crystal lattice to the right.

Crystalline structures contain many lattice planes. A lattice plane is any plane that contains at least three linearly independent lattice points of a material. Since the crystal is periodic, all lattice planes are also periodic and build up a collection of equally spaced parallel lattice planes that together intersect all lattice points. Miller indices are used as a notation system for the planes. To denote a family of parallel lattice planes three integers are used, commonly written (hkl), which is equivalent to the normal vector of the crystal plane that is indicated [8]. Examples of Miller indices of different crystal planes are presented in Figure 2.2.

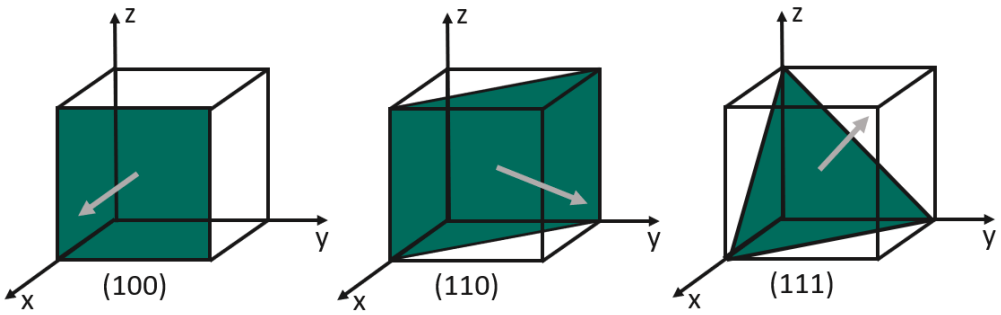

Figure 2.2: Unit cells with crystal planes of different Miller indices marked in green. The vector that is perpendicular to the crystal planes are shown with gray arrows.

The crystal lattice builds up the whole crystal, but there are both defects and edge effects to take into account. No crystal can be infinitely large, the lattice pattern therefore deviates at the edges. Still, a crystal is usually comprised of a large number of unit cells, which means that the edge effects will be small compared to the crystal as a whole. Defects in a crystal are inevitable and there can be both defects in the form of impurities as well as vacancies or extra atoms in the lattice. To describe the principle of diffraction and scattering it is however assumed that the crystal is ideal and there are no defects or edge effects to consider [9].

As opposed to crystal structures with long-range order there are also amorphous materials which do not display any long-range ordering. The structure of an amorphous material can be considered as atoms with positions that are equally random as atoms in a liquid. The difference to a liquid is however that the amorphous material contains atoms that are unable to move. There is no unit cell since the structure does not repeat itself and two positions far away from each other typically shows no correlation. There can however still be short-range order in a material, which means that on a short distance there is correlation between how the atoms are arranged, as shown in Figure 2.3 [8].

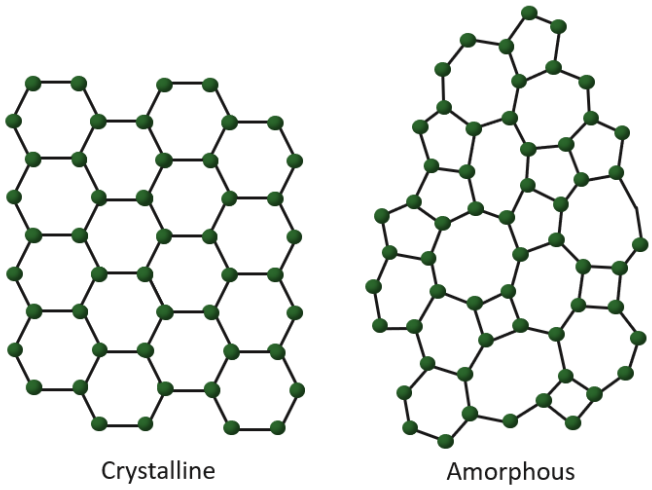

Figure 2.3: A crystal (left) has both short-range order and long-range order, while an amorphous material (right) has short-range order, but no long-range order.

2.1.2 Scattering and Braggs Law

Scattering includes a wide range of physical phenomena when photons or other particles in motion are forced to deviate from their trajectories when passing through a medium due to interactions with the atoms in the material. Scattering is a widely used phenomena in material characterization since the scattering pattern from a material yields information about the structure. If the incoming beam consist of photons, scattering may be a non-destructive method [10].

Mathematically, scattering from an incoming photon beam in a crystalline sample can be modelled with Braggs law, as in Equation 2.1.

$$n\lambda = 2d_{hkl}sin\theta \tag{2.1}$$

where λ is the wavelength of the light, d_{hkl} is the distance between the (hkl)-planes of the material, θ is the angle of the incoming light and n is a positive integer. In a crystalline material, atoms will scatter the incoming beam with an angle as a result of the repeating structure of the material, see Figure 2.4. Figure 2.4 shows the scattering in two dimensions, but most materials have a structure in three dimensions. The scattered beam forms a scattering pattern that, for example, yields information about the distance between atom planes in the material. Scattering is a three-dimensional event in three-dimensional materials, so Figure 2.4 only shows a two-dimensional simplification of the phenomena.

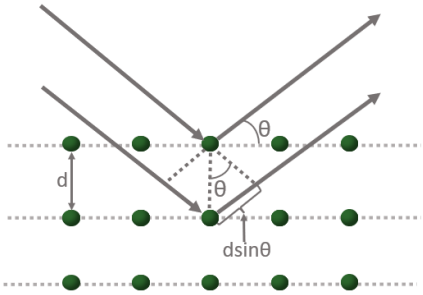

Figure 2.4: Incoming photons scatters from the crystal lattice in an angle θ.

2.1.3 Theory of Small- and Wide- Angle Scattering

SAXS and WAXS are non-destructive scattering techniques used to establish general structural features of systems. The difference between the two methods is related to the size of the scattering angle, as can be understood by their names; *small*-angle X-ray scattering and *wide*-angle X-ray scattering. SAXS and WAXS can be used to investigate structures with typical sizes from a few Ångstrom up to micrometers [11].

Figure 2.5 shows a SAXS or WAXS experiment where an X-ray beam is hitting a sample and the transmitted X-rays hit a detector. A part of the light change direction due to scattering. A considerate amount of the X-ray light is not affected by the sample and will merely pass through. To protect the detector from the strong beam a device called a beam stop is used to shield the detector. The detector is hit by scattered photons to produce a scattering pattern. The placement of the detector is different for SAXS and WAXS, where the former is further away and the latter is closer, to detect different scattered angles [8].

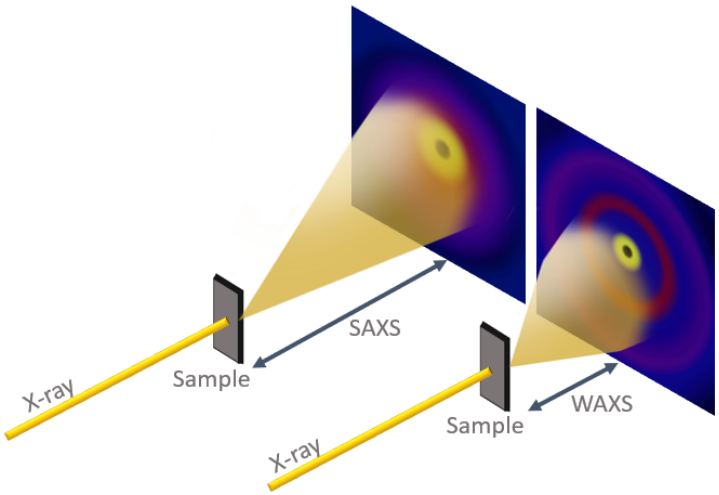

Figure 2.5: The setup of a SAXS and a WAXS experiment respectively. The detector is moved further away from the sample to catch the small angle scattering for a SAXS experiment, and moved closer to the sample to catch the larger angle scattering for a WAXS experiment.

An incoming photon beam will scatter due to the repeating structures in the material, and form a scattering pattern on the detector. An interference pattern of constructive and destructive interference is therefore produced, and information of the structure of the material can be deduced. A vector, commonly denoted q, is used to quantify the interference pattern [12]. The vector q is related to a vector between the incoming beam and the scattered beam as, $q = k_f - k_i$, and depicted in Figure 2.6.

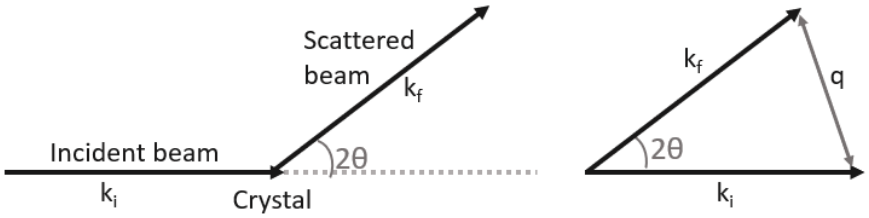

Figure 2.6: The incoming beam is characterized by a vector k_i, while the scattered beam is characterized by the vector k_f, and has deviated in an angle of 2θ. The difference between k_i and k_f is denoted with the vector q.

Scattering angles, θ are usually smaller than 0.1°, which means that the small angle approximation, where $sin(\theta) = \theta$, can be used. A relation between the q-value of the interference and the size of the structure which lead to the scattering pattern can be found by Equation 2.2.

$$d = \frac{2\pi}{q} \tag{2.2}$$

In Equation 2.2; q is the absolute value of the q-vector, and d is used to determine the distance of repeating structures in the material. Typical scattering patterns for polymers are presented in section 2.4 after the structure of the polymers has been described.

2.2 Polymers

The definition of a polymer is a large molecule constructed of smaller repeating units called monomers covalently bonded together. A subgroup of polymers are plastics which are defined as organic polymers capable of changing their shape. Plastic materials can be formed into complex shapes by applying pressure or heat, they are therefore moldable and malleable [13].

2.2.1 High Density Polyethylene, HDPE

The main focus of this work is the plastic material high density polyethylene, or HDPE, since it is highly used in the packaging solutions of Tetra Pak®. Polyethylene is a polymer of the monomer ethylene, see Figure 2.7.

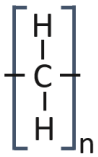

Figure 2.7: The monomer of HDPE. The n is a positive integer, and denotes that this monomer can bind to several similar structures, hence forming the carbon chain of HDPE.

There are several compositions and structures of polyethylene since the monomers can attach to each other and build chains in several configurations, which will be explained thoroughly in section 2.2.3. It was first produced in 1922 from a lab experiment gone awry and has since then grown to become the polymer synthetically produced in the largest volume on earth. HDPE is distinguished from other polyethylene material by its density and the Society of the Plastics Industry identifies high density polyethylene as a polyethylene with a density in the range of 0.941-0.965 g/cm^3 [14].

Polyethylene is used for packaging because it is a thermoplastic material. It can be melted and shaped into desired format then be subsequently remelted and shaped into other forms. This is not only advantageous from a recycling perspective, where the plastic parts of packaging can be reused, but also from a production perspective. HDPE is produced as pellets and can at the packaging factories be reshaped into requested structure by melting. Polyethylene is economically advantageous to use since it is the cheapest of the major synthetic polymers. Furthermore, it has excellent chemical resistance which is beneficial in the food industry where the quality of the food must be guaranteed [14].

2.2.2 Injection Molding

Injection molding is a process where solid plastic is melted, injected into a mold and then cooled to once again form a solid. Since HDPE is a thermoplastic material that can be molten and cooled several times, injection molding is one of the appropriate methods to shape the material. A schematic image of an injection molding apparatus is presented in Figure 2.8.

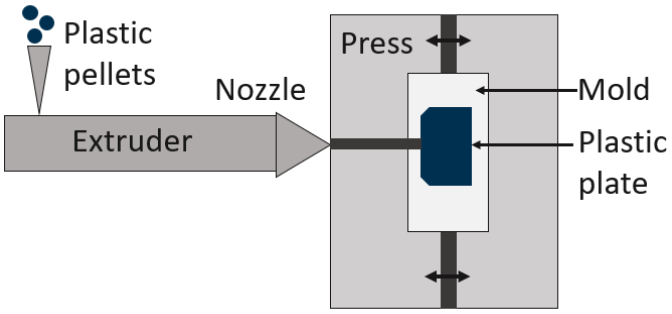

Figure 2.8: Schematic of the injection molding process.

The process begins with plastic pellets continuously supplied into the extruder, where the material slowly is being heated and sheared. The inside of the extruder consists of a screw-like device that on the one hand melts the material until liquid and on the other hand pushes the material forward in the screw closer to the nozzle. The melted plastic accumulates and the end of the extruder, thereafter it is injected by the screw, at high pressure, into the nozzle and subsequently into the mold. Cooling of the hot plastic takes place in the mold, which is held together by a high clamping force, to ensure the shape of the mold. After sufficient cooling time, the clamping force is released and the plastic can be ejected from the mold [3].

Due to different flow properties and cooling rates the plastic will not have a uniform structure over the entire mold. The flow of the melted polymer and formation of its layers are depicted in Figure 2.9.

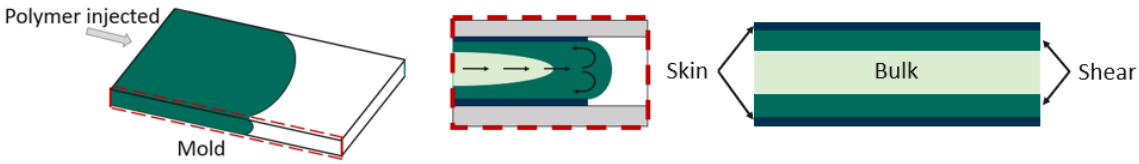

Figure 2.9: A schematic the effect of the flow on the layers of HDPE. The injection of HDPE into the mold leads to a flow that rapidly cools down closes to the cool mold edges, called skin. The subsequent shear layer is sheared between the skin and the rest of the material, while the bulk layer is allowed to cool relatively undisturbed.

After injection the plastic is cooled by the walls of the mold. The material that is in direct contact with the walls will therefore cool rapidly creating a so-called skin layer. The heat transfer through the skin layer is not as rapid as from the mold to the skin resulting in a heat gradient from the skin layer into the middle of the material. The material closest to the skin will partly cool down while still being sheared of the moving material in the bulk. Another layer with distinctive structure is therefore formed, the so-called shear layer. The middle part of the flow will be less affected by direct cooling from the walls or shearing by the skin layer and is called the bulk layer [15].

2.2.3 Morphology

Although polyethylene is defined by its monomer, it comes in bewildering many compositions and arrangements. It can have different molecular weights and different microstructures, depending on the polymerization process and molding production [14]. The structure of the material plays a central part in its characteristics and plasticity. HDPE show a hierarchical morphology, meaning that it displays a typical structure on different length scales [16]. As mentioned, in the case of HDPE, the monomers create linear and branched chains, which in turn can arrange in larger crystalline or amorphous structures.

2.2.3.1 Crystalline and Amorphous Regions

HDPE exist as a semi-crystalline material, which contain both crystalline and amorphous parts. The reason for the crystallization has to do with the interplay between the entropy and the internal energy of the system. The Gibbs free energy is given by the well-known equation presented in Equation 2.3:

$$G = (U + PV) - TS \tag{2.3}$$

where G is Gibbs free energy, U is internal energy, P is pressure, V is volume, T is absolute temperature and S is entropy of the system. When crystallizing, the polyethylene chains arrange in an ordered pattern, which is associated with a large negative change of entropy. To have a favorable free-energy change, i.e minimize the Gibbs free energy, the negative entropy has to be balanced by a negative internal energy contribution. In a disordered state the polymer chains are highly entangled with little available volume to move freely. Many chain configurations are therefore trapped in a conformational state with higher energy than a relaxed state. When forming a crystalline system, the chains adapt an arrangement of rotational states of lowest energy. The balance between the decreased entropy and the decreased energy decides the amount of crystallization, and hence also the amount of amorphous material [13].

As mentioned, crystalline materials can be described by a unit cell, which is true for HDPE as well. The unit cell of HDPE is presented in Figure 2.10. The chains are held together by covalent forces, while the interaction between chains is dominated by van der Waals forces [7].

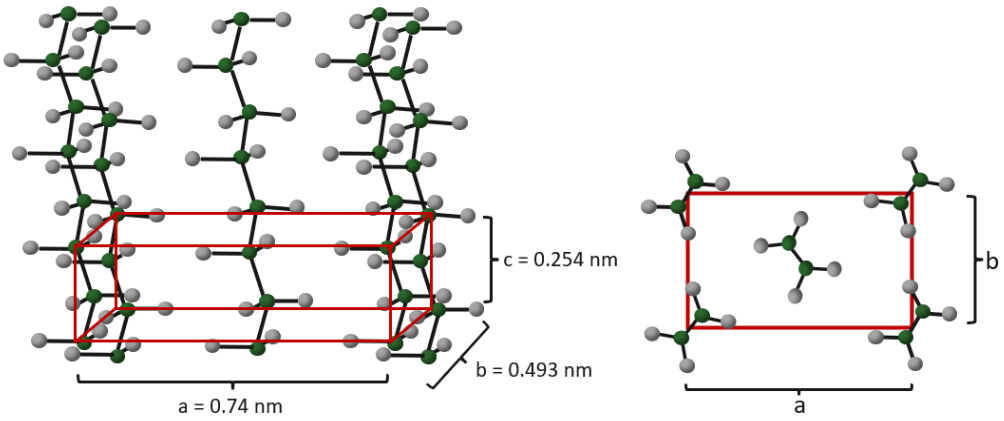

Figure 2.10: The chains of HDPE align to form a crystal. The unit cell with corresponding lattice parameters of the crystal is marked in red.

There is an unlimited amount of crystal planes in the crystalline structure of HDPE. The crystalline parts of HDPE typically arrange themselves in lamellae. The thickness of these ranges from 5 to 25 nm and the lateral dimension ranges from 1 to 50 μm. In between the lamellae there are regions with polymer in amorphous arrangements [7], as shown in Figure 2.11.

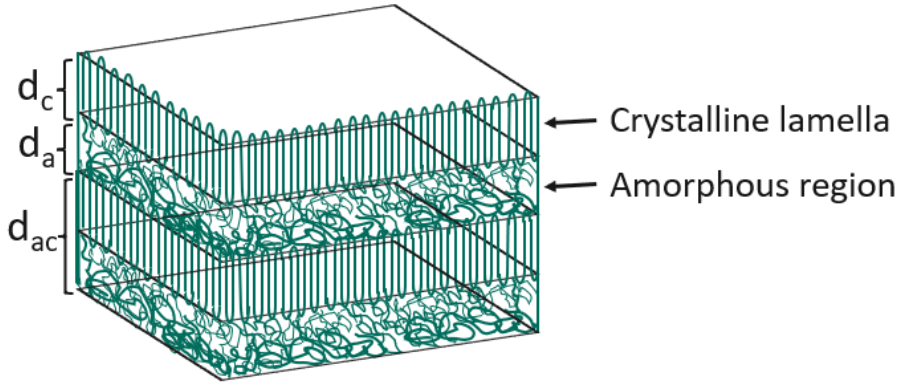

Figure 2.11: HDPE orders in crystalline and amorphous parts. The thickness of the crystalline lamella is denoted d_c, the thickness of the amorphous region is denoted d_a, while the thickness of one lamella and one amorphous part is denoted d_{ac}.

2.2.3.2 Spherulites and Shish Kebab Structure

As mentioned, HDPE has a hierarchical structure; the ethylene molecules covalently bind together as chains, the chains create crystalline lamellae surrounded by amorphous parts. These lamellae can further create even bigger partly ordered structures in the form of spherulites and shish kebab [17].

A spherulite is a spherical semi-crystalline structure, where the previously mentioned HDPE lamellae are connected to each other through amorphous regions in-between

the lamellae within the spherical structure. The lamellae then grow outwards to form the spherical shape, as represented in Figure 2.12 [18]. The size of the spherulites generally depend on the cooling rate of the polymer and are usually on the order of 100 μm in diameter [7]. The spherulites are not necessarily completely symmetrical, and can adapt more elliptic and oblong shapes, especially if the polymer is deformed by flow during formation [19].

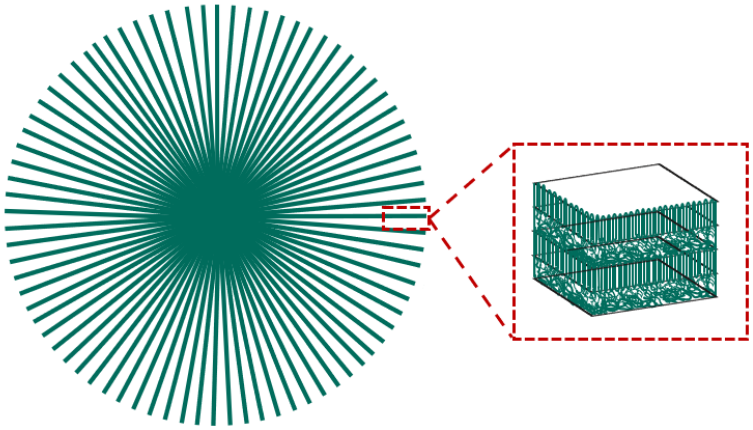

Figure 2.12: Depiction of a spherulite. The regions of crystalline and amorphous layers grow from the nucleus outwards. The spherulite schematic is depicted in 2D for simplicity, but the spherulite is actually a 3D structure.

When the polymer is a subject of high flow and rapid cooling the polymers tend to align with the flow and form the shish kebab structure instead of spherulites, see Figure 2.13. The shish kebab structure consists of a long central shish core surrounded by lamellar crystalline kebab structures periodically attached to the core. The alignment of the chains leads to high strength of the material, for injection molded polymers this is typically the structure of the material in the skin layer [20]. The mechanism of the formation of shish is still not fully determined [21].

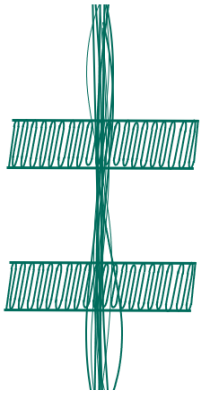

Figure 2.13: The shish kebab structure contains a fiber-like core with perpendicular crystalline lamellae.

2.2.4 Structural Change During Plastic Deformation

The previously described structures exists mainly in undeformed HDPE. In packages, the material can be exposed to certain forces, for example pressure or traction. To test the strength of the material, it is often stretched. The elongational deformation of the polymer leads to changes in the structure. Deformation begins with change of the amorphous parts of the structure. The unordered structures can under force detangle, and for large forces a phenomenon called cavitation may take place, where voids in the material are created. These effects only happen during tension, not during compression or shearing [22].

Further deformation involves the crystalline parts and there are many types of crystalline deformations, for example; the chains can move vertically against each other in chain slip, or the lamellae starts moving in lamellar shear [23]. One type of crystalline deformation that can take place is the martensitic transformation where the unit cell of the polyethylene changes to counteract the applied strain in the material. When the force is removed, the structure can go back to the original unit cell. The unit cell changes from the usual orthorombic, as presented in Figure 2.10, to a monoclinic one, as described in Figure 2.14 [24, 19].

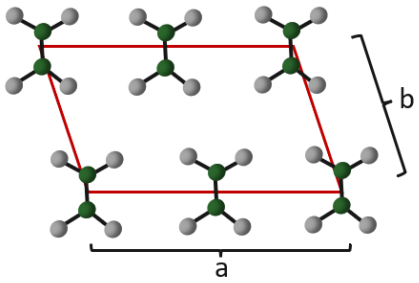

Figure 2.14: A depiction of the monoclinic unit cell of HDPE. The dimensions of the unit cell are different from the orthorombic one with lattice parameters a=8.09 Å, b=4.79 Å and c=2.53 Å.

The behavior of spherulites under applied stress is an important factor in understanding how HDPE deforms. There are two types of deformation mechanisms for spherulites; homogeneous, and inhomogeneous. In homogeneous deformation the spherulites are elongated and when deformation stops, the spherulites can return to the original confirmation. The material is therefore elastically deformed, with the possibility of regaining the original shape. For inhomogeneous deformation, the middle part of the spherulite also stretches without the possibility of regaining its original structure, see Figure 2.15 [7].

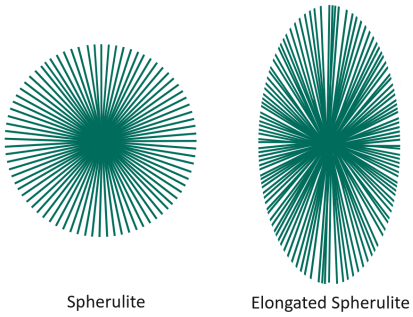

Figure 2.15: Spherulites can either be completely spherical (left structure) or slightly elongated to an ellipsoidic structure (right structure).

Further deformation of the spherulites will lead to microfibrillation. During deformation of spherulites the material will first experience cavitation, or voids between the lamellae, but also fragmentation of the material. Fragmentation means that the material breaks apart to form smaller crystalline blocks where chains are pulled out to form densely-packed microfibrils, as shown in Figure 2.16 [19].

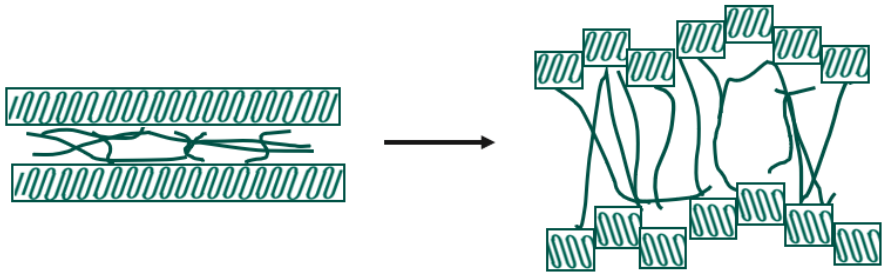

Figure 2.16: When the material is subject to force the lamellae will be torn apart into crystalline blocks and form microfibrils.

2.3 Mechanics of Polymers

Previous section described the deformation of HDPE on a nano- or micrometer scale. To explain the mechanics of polymers it is necessary to zoom out further and look at the material as a whole. Plastic materials are generally elastic materials (regain their original shape if the shape is distorted) up to a certain deformation where the material cannot regain their shape [13].

To quantify the elastic properties tensile testing can be used. The setup of tensile testing is relatively simple. It consists of two fixtures where the sample is clamped in place. The sample is in a so-called dog bone shape, which is wider at the ends to get enough area for the tensile tester to grip, while the intermediate part is thinner so that the deformation process happens in the middle. The fixtures can move by an applied force in order for elongation of the test specimen at a constant strain rate. The corresponding stress of the material is measured [8]. The setup of a tensile test is presented in Figure 2.17.

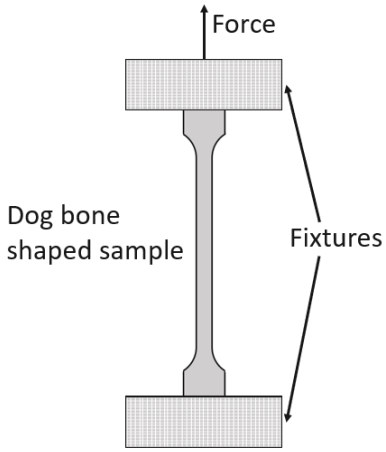

Figure 2.17: The dog bone shaped sample is clamped in place by the fixtures. An applied force stretches the sample, while the stress and strain are measured.

Tensile testing is a destructive deformation process providing information about the tensile strength and yield strength of the material. At low stress the lamellae can easily separate. The amorphous parts in between lamellae can detangle and stretch, which will give total recovery when the external stress is moved, this is called the elastic region. At higher stresses the first yield point is reached. The material can no longer recover and the structures within the samples permanently deforms. A typical stress-strain curve is presented in Figure 2.18, where the yield points and tensile strength are marked.

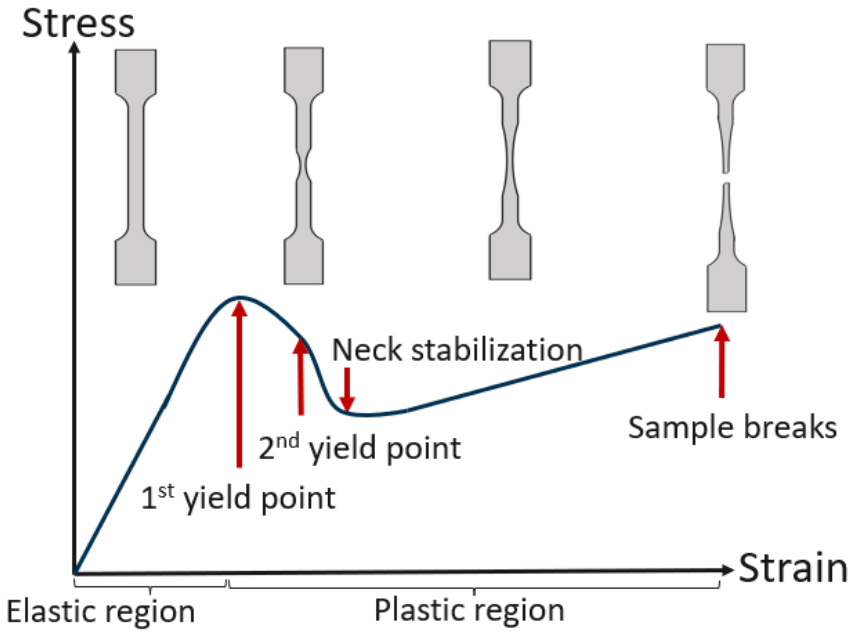

Figure 2.18: Typical stress-strain curve from a tensile test experiment. The 1st and 2nd yield point as well as the breaking point of the sample is marked.

After the first yield point the material goes through necking, where a thinning of the material can be observed. The structural change during necking often includes orientation of the previous unoriented lamellae aligning with each other to form a more oriented structure. Cavitation is also likely to happen during necking [19]. Cracks and cavities in between the lamellae lead to the material whitening and thinning, which can also be observed for the sample during necking [8]. Many elastic materials only show one yield point.

In the case of HDPE, a second yield can be observed in tensile experiments. At the second yield point there is a considerable change in the structure of the material. The spherulitic structure is transformed into a microfibrillar structure when the lamellar blocks are torn apart from each other [25]. The necking then continues throughout the material, where more and more material is being pulled into the neck, while the structure of the already necked materials stays the same. At one point there is no more material to draw into the necking and the sample will break. The strength needed to completely break the material is called the tensile strength.

During this work, less focus has been placed on the quantity of the yield strength and tensile strength, while the main focus has been on the qualitative behavior of the material at the two points. The yield stress has been found to be proportional to lamellar thickness and at constant molecular weight the yield stress increases with percentage of crystallinity in the material [26, 17]. The microscopic behavior the HDPE structure can therefore be linked to the macroscopic behavior during tensile testing.

2.4 Typical Polymer Scattering Patterns

Both the basic principle of X-ray scattering and the microscopic behavior of the HDPE structure has been described, and it is of interest to connect the two areas to comprehend the results of this work. As mentioned, the difference between SAXS and WAXS is the detector distance from the sample, hence which angle of scattering that is detected, which in turn corresponds to different characteristic length scales in the material.

WAXS typically detects structures on the order of nanometers. In HDPE this would correspond to the distance between crystal planes in the lattice, as shown in Figure 2.19.

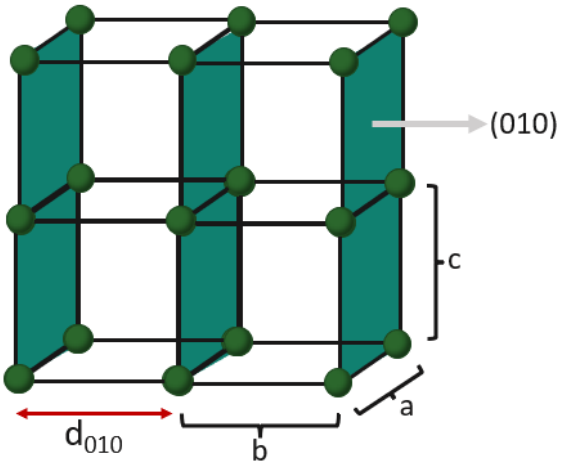

Figure 2.19: The (010) planes can be seen in the crystal lattice, with lattice parameters a, b, and c, in green. The distance between the planes is thus denoted d_{010}.

The theoretical distance between the lattice planes can be calculated, since the unit cell is known as well as the lattice parameters. The distance between different crystal (hkl) planes can be calculated as in Equation 2.4:

$$d_{hkl} = \frac{1}{\sqrt{(\frac{h}{a})^2 + (\frac{k}{b})^2 + (\frac{l}{c})^2}} \tag{2.4}$$

where hkl are the Miller indices of the crystal plane in question and a, b, and c are the lattice parameters of the unit cell. The data from a WAXS experiment can be used to obtain the distance between the (hkl) planes by finding the peak positions and using Equation 2.2 to find d_{hkl}, as shown in Figure 2.20.

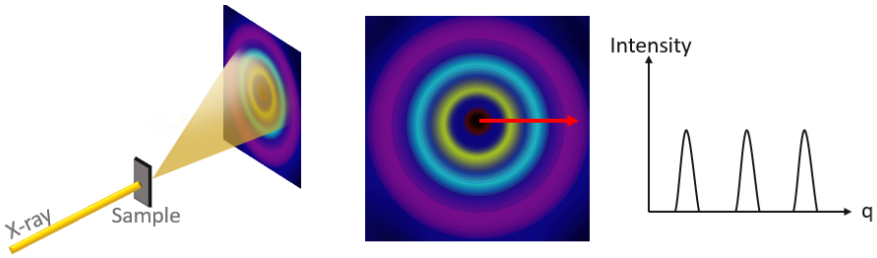

Figure 2.20: The SAXS or WAXS pattern can show a symmetrical pattern. To reduce the data to a graph, the intensity of the pattern is integrated from the center of the detector and outwards, shown with a red arrow. This leads to an intensity plot that shows the intensity of the scattering as a function of q.

The scattering from the crystal planes takes place in all directions, which creates a scattering pattern on the detector. WAXS experiments of HDPE the patterns typically show rings corresponding to scattering from the different (hkl) planes. To find the q-value of the peaks the data can be integrated radially to form a plot of q-value vs intensity. By using Equation 2.2, the theoretical distance between the

peaks can be determined. Figure 2.20 depicts the peaks, while previous work of HDPE carried out by Butler et al. [19] shows actual WAXS patterns and radially integrated data, as shown in Figure 2.21.

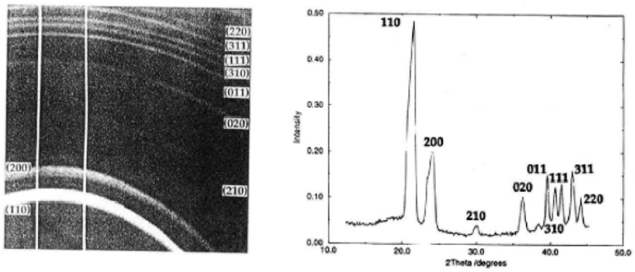

Figure 2.21: Previous work from Butler et al. [26] shows the WAXS pattern and the corresponding intensity plot. Since the pattern is symmetric, only a small part of the scattering pattern is shown.

The peaks from the different crystal planes in Figure 2.21 are not equally intense since the occurence of parallell planes are higher for planes with low values of (hkl). There are therefore less parallell planes of planes with high values of (hkl) and the scattering intensity of these are lower [26].

The (110) peak in WAXS, corresponds to the undeformed orthorombic crystal structure of HDPE. When it is exposed to stress, the unit cell changes through the martensitic transformation. The transition leads to a change in the scattering pattern and can be distinguished by a decrease of the intensity of the (110) peak of the orthorombic unit cell, while there will be an increase of a (001) peak of the monoclinic unit cell. The (001) peak gives rise to a peak located at lower q-values [19].

SAXS-patterns can be analyzed similarly to WAXS patterns, but identifies structures on a larger scale. The peaks correspond to characteristic distances in the material. For HDPE, the characteristic distance would correspond to the mean distance of one lamella together with the region of amorphous chains, denoted d_{ac} in Figure 2.11.

Scattering produces diffuse halos on the detector as shown in Figure 2.21. However, the scattering pattern is not always symmetrically distributed around the middle. A significantly oriented structure, as in the case of the shish kebab structure, which have many polymer chains aligned in one direction in the material, will show a scattering pattern that is highly asymmetrical, see Figure 2.22 [13].

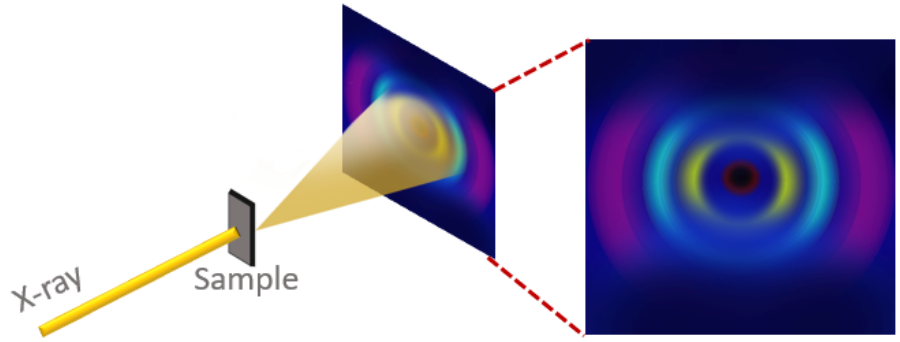

Figure 2.22: A structure that is asymmetric will lead to a pattern that is asymmetric.

When interpreting SAXS patterns, the rule is that the more symmetrical pattern, the more randomly oriented structures in the material, and vice versa, the more asymmetrical patterns the more aligned structures.

SAXS and WAXS are widely used techniques to study plastic material. The scattering patterns that are created from the previously described structures are characteristic for respective structure and can be used for identification. The indicative scattering patterns for the spherulite, elongated spherulite and a shish kebab structure are depicted in Figure 2.23 [21, 27].

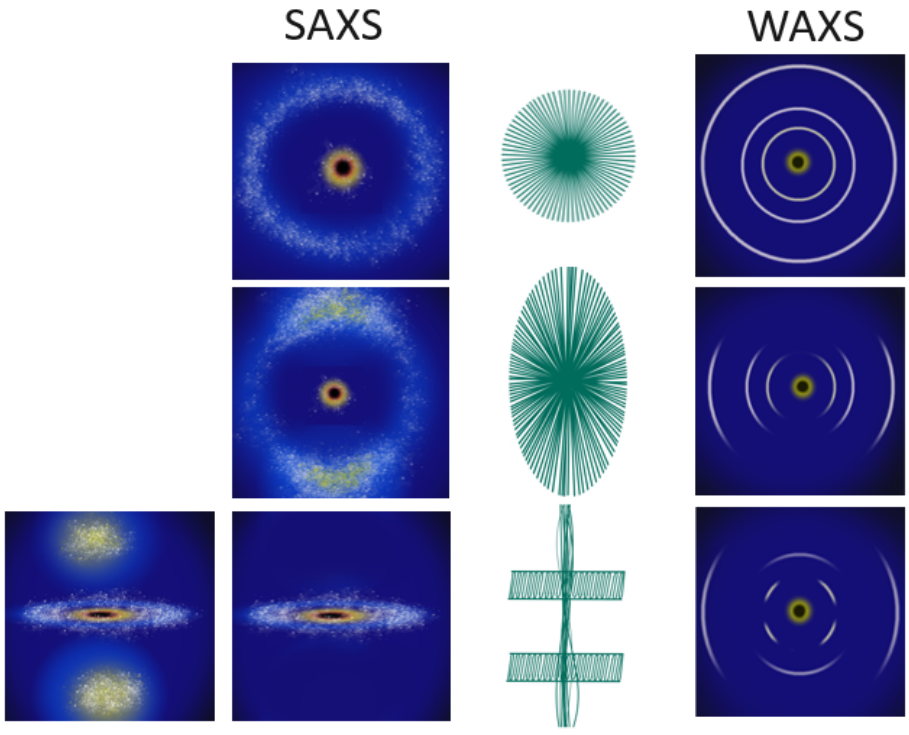

Figure 2.23: Typical SAXS and WAXS patterns from spherulites, elongated spherulites and the shish kebab structure [21, 27].

Figure 2.23 shows that the spherulite typically shows a very symmetric pattern, due to the symmetry of the spherulite itself. The elongated spherulie however shows a more oriented structure, with regions of higher intensity. The shish kebab structure can show different scattering patterns depending on from what direction it is viewed. Similar for SAXS and WAXS patterns are however the oriented elongated scattering pattern.

3
Methods

3.1 Sample Preparation

The first step of the investigation was to produce the polymer to be used for further experiments. Preparation of all samples was performed at Tetra Pak® in Lund. HDPE of density 0.953 g/cm^3 with a Melt Flow Index of 26 g/ 10 min was used in the procedure. A standard injection molding machine, i.e an Arburg 470 800-70S hydraulic injection molding equipment was used to produce test plates following ISO 294-5. The plastic melt, with a temperature of 260°C, was injected with a volume flow of 25 cm^3/s into the equipment, with a temperature of 60 °C. The point at which the volume-controlled injection was switched to a pressure-controlled holding at a 85% cavity filling ratio. The holding pressure was held for 1 second, decreased linearly from 900 to 750 bar, with pressure levels chosen to obtain an even thickness of 0.6 mm over the plates. Holding pressure was followed by cooling for 11 seconds. The dimensions of the prepared plastic plate is presented in Figure 3.1.

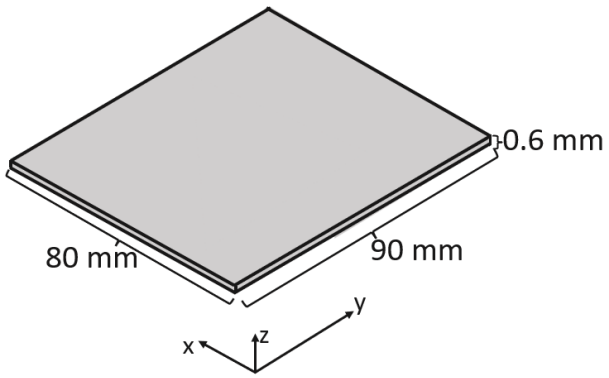

Figure 3.1: Schematic illustration of the plate sample (ISO standard: ISO 294-5).

As mentioned, the polymers will not have a uniform structure over the entire plate. To investigate the anisotropy samples were cut from the plates in ways described in the following section.

3.1.1 Tensile Specimen

Tensile testing required samples that were shaped as dog bones. The shapes and sizes of the dog bones studied post-mortem followed the ISO standard of 527-2 1BA, with dimensions described in Figure 3.2.

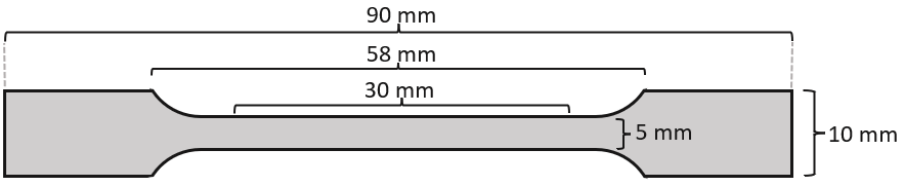

Figure 3.2: Dimensions of the dog bones of ISO standard 527-2 1BA.

These were cut out from the samples in two directions. The machine direction, or MD, follows the flow of the polymer into the mold. The cross direction, or CD, was cut out in the direction perpendicular to the flow, as seen in Figure 3.3

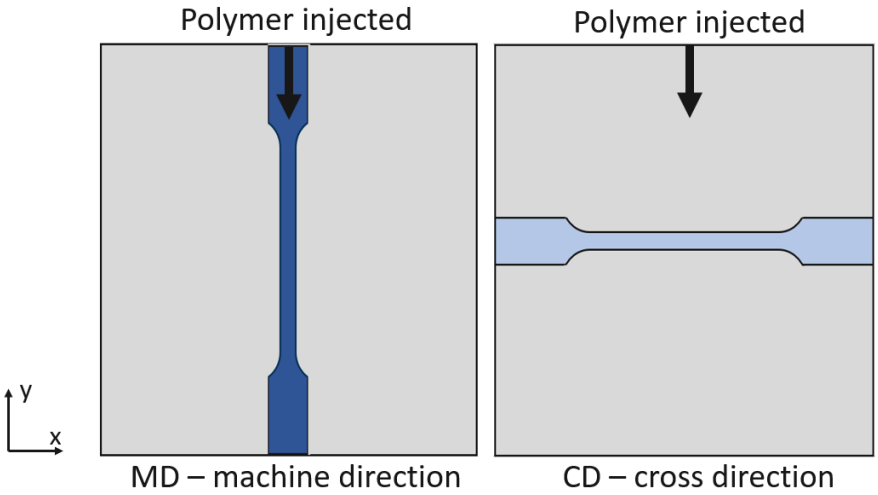

Figure 3.3: Depiction of how the MD and CD samples were cut from different HDPE plates.

As mentioned in the theory section above, the polymer structure is arranged differently for the skin, bulk and shear layer, more specifically the z-direction, as described in Figure 3.4. To investigate these different layers, several polymer plates were ground to obtain samples that only contained a single layer. The thickness of the layers was measured using polarized optical spectroscopy. CD specimen were cut out and mounted onto a holder by heating the holder to 55°C. Bee wax, with a melting temperature of 45°C, was attached to the specimen. Grinding was performed manually using a wet p120 sandpaper with cooled water to reduce friction. To improve surface finish, a Penta 5000 hand grinder was used, with a final grinding of p2000. Test plates of the shear and bulk layer were obtained, while the skin layer was too thin to isolate.

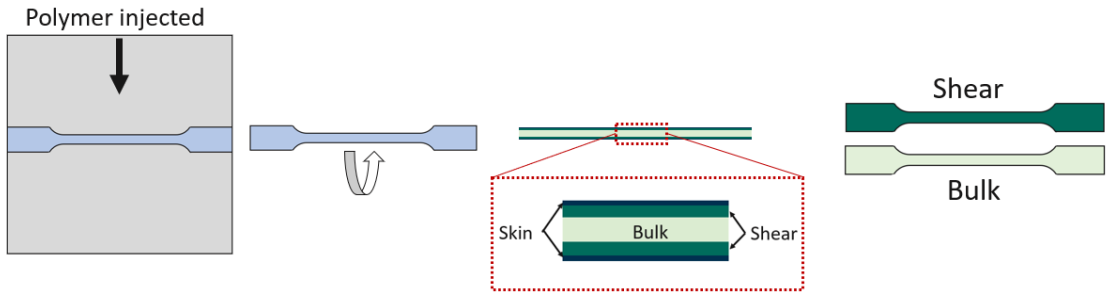

Figure 3.4: The plates were ground to only contain either the shear layer or the bulk layer. Dog bones of the samples were thereafter cut out.

The undeformed, original samples were investigated in this work, but the aim was also to investigate what happened to the material during deformation. Tensile testing was used to obtain deformed samples. Tensile testing was performed in the machine Zwick Z010 Proline with a load cell of 1 kN, at ambient temperature and a displacement rate of 100 mm/min.

The samples were stretched until rupture. Each half of a broken dog bone contains; grip, neck, and tip. The grip region is less deformed during tensile testing, while the neck was significantly elongated and ruptured at the tip, as presented in Figure 3.5.

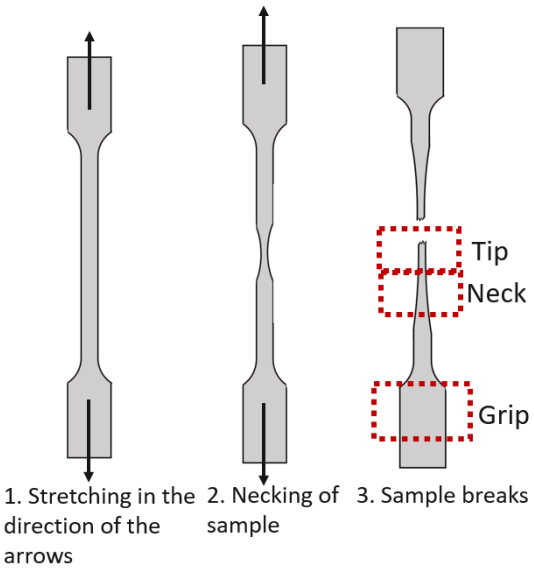

Figure 3.5: The different stages of the dog bones during tensile testing. The dog bone is initially stretched (1) until the yield point is reached and necking begins (2), the necking continues to grow throughout the sample until the force is too big and the sample breaks (3). Three different parts of the samples were investigated in this work, the tip, the neck, and the grip, all marked in red.

The tensile testing was perrformed at Tetra Pak® in Lund. The deformed dog bones were then sent to Chalmers to be prepared for SAXS and WAXS measurements.

3.2 SAXS and WAXS

Several samples were investigated at the Swiss Light Source, SLS, at Paul Scherrer Institute (PSI, Switzerland). A synchrotron is an X-ray beam of high brilliance that gives fast investigation and high resolution. The samples were measured at PSI during two different occasions. The samples of full thickness deformed in the MD and CD direction were measured on beam time 1, while the samples of the separate layers were measure on beam time 2.

All the samples were mounted on sample holders to perform SAXS and WAXS experiments. During tensile testing, the sample may break closer to the undeformed part than in the middle, this leads to different lengths of the samples that were used. For MD and CD, the whole sample could be scanned during one measurement while for the layers shear and bulk the separate parts (undeformed, neck and tip) were measured during separate scans, see Figure 3.6.

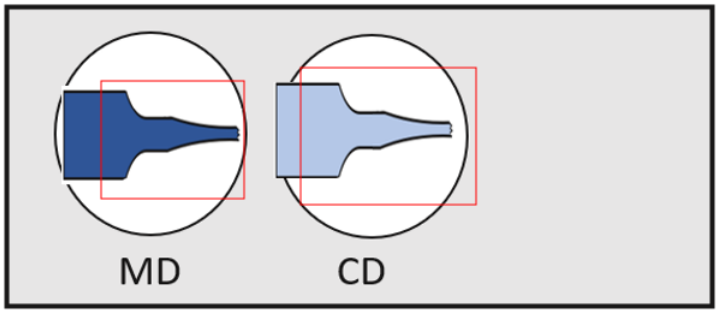

Sample	FOV [mm]
MD	6.51x5.64
CD	8.01x6.51

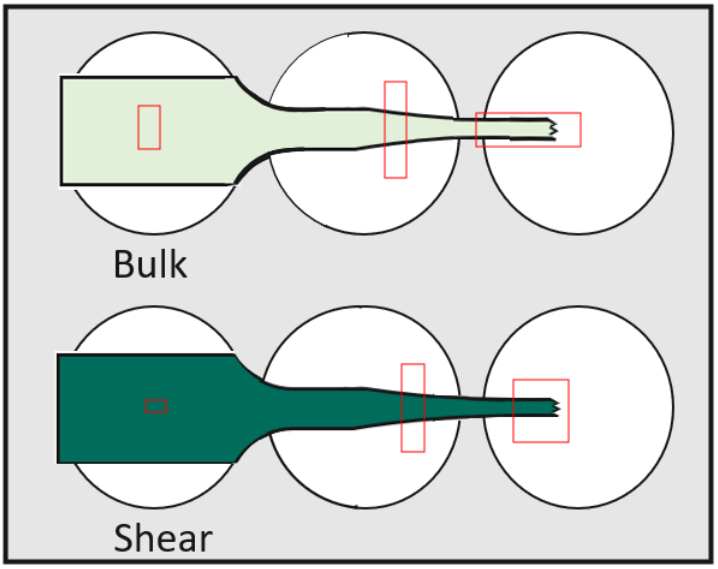

Sample	FOV [mm]
Grip	2x1
Neck	4.38x1
Tip	1.5x5

Sample	FOV [mm]
Grip	0.5x1
Neck	4x1
Tip	2.5x3

Figure 3.6: The samples were mounted on the sample holder in gray, the holes in the sample holder is the areas from where the X-ray beam is shone so that the scattering pattern can be obtained. Scans of CD and MD used shorter samples than shear and bulk. The area that was measured, or field of view (FOV), is marked with red boxes.

Both measurements utilized a Si(111) double crystal monochromator and X-ray energy of 12.4 keV, and a Pilatus 2M detector was used. The measurements of CD and MD had a distance of sample to detector for the SAXS measurements of 2171 mm and the WAXS measurements of 250 mm. An exposure time of 0.06 s and an X-ray beam focus of 42x4 μm was used. For the shear and bulk samples, the distance of sample to detector for the SAXS measurements were 7107 mm and for the WAXS measurements 237 mm. The exposure time for SAXS was 0.05 s and 0.10 s for WAXS. The X-ray beam was focused to 24x51 μm.

3.3 In-situ SAXS and WAXS

Several samples were investigated with SAXS and WAXS in-situ at Empa, Center for X-ray analysis in St. Gallen, Switzerland. The in-situ tensile testing required dog bones of smaller sizes, since the tensile stage was small enough to fit inside the SAXS instrumentation. The dimensions of the smaller dog bones are described in Figure 3.7. This dog bone version was not intended to use for tensile tests, but mainly for tensile impact experiments. The dimensions however coincide with what was needed for the tensile stage and the narrow waist of the sample was advantageous to get necking in the exact middle of the sample, justifying use in these experiments.

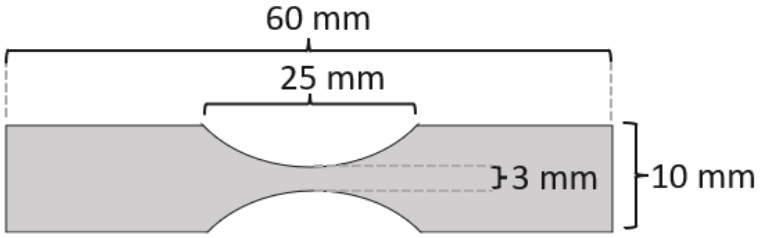

Figure 3.7: Dimensions of the dog bones of ISO standard 8256.

The samples were mounted in the tensile stage (Anton Paar, TS600) and pulled with the continuous rate of 1 mm/mm until 14 mm extension. The sample was released with the same rate until it reached the initial state. This took place simultaneously as the measurements of SAXS and WAXS.

The scattering measurements used a NANOSTAR system (Bruker AXS GmbH, Karlsruhe, Germany). A 2D MikroGap technology-based detector was used and the X-ray source produced an X-ray beam from CuKα with wavelength 1.54 Å. The scattering patterns were recorded at room temperature under moderate vacuum conditions, to limit air scattering. As the tensile stage continuously was in action the scattering patterns were collected with an exposure time of 10 seconds. The sample to detector distance for WAXS and SAXS experiments were 144.5 mm and 1070 mm, respectively.

The MD and CD samples were investigated in-situ with both SAXS and WAXS. The shear and the bulk samples were too thin to be investigated by this setup. The fixtures of the tensile stage were too tight and made the thin sample break close to the fixtures instead at the middle of the sample. The elongation and necking of the shear and bulk separately could therefore not be investigated.

3.4 Processing of Data

As mentioned in the theory section the, SAXS and WAXS patterns corresponds to structures in the material. During a SAXS or WAXS experiment performed at a synchrotron source, the sample position can change, making it possible for the beam to scan the whole sample. The scanning SAXS or WAXS thus yields a scattering pattern for each point that has been investigated.

Instead of examining the patterns from every single point of the sample, the data can be reduced. The data can be integrated from the center outwards to larger angles, giving information about the characteristic distances within the sample, as described in the theory section. The radial integration is affected by asymmetry of the scattering pattern, as shown in Figure 3.8.

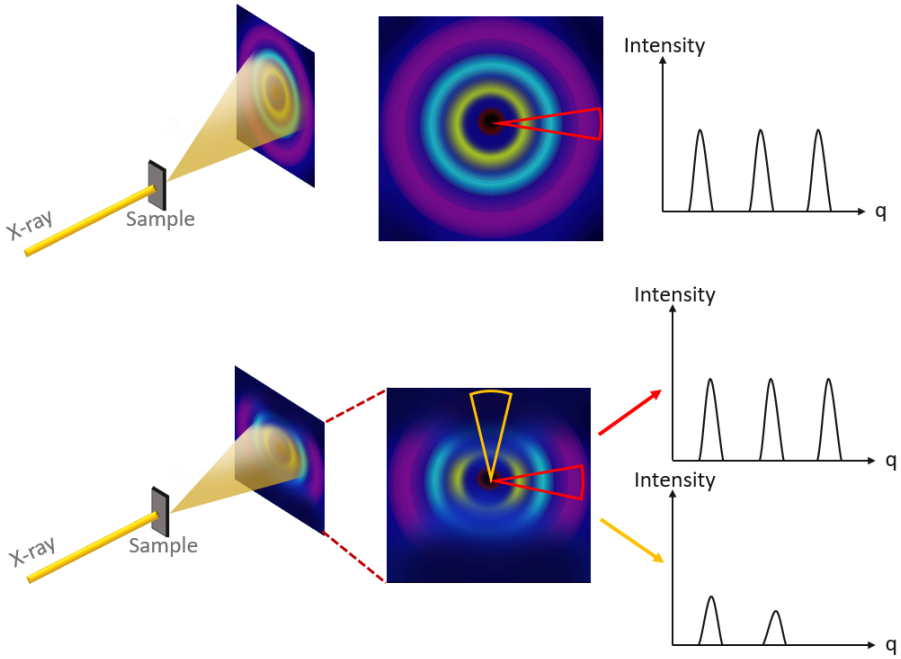

Figure 3.8: The upper figure shows a symmetric scattering pattern. Radial integration will yield similar peaks, no matter in which direction it is takes place. The lower figure shows an asymmetric scattering pattern. Radial integration will yield different peaks depending on in which direction the integration takes place.

According to Figure 3.8, the radial integration depends on in which direction the integration is taking place due to the asymmetry. To find an estimate of the alignment,

or orientation, of the structures in a material, this asymmetry is important. The data from the patterns can be reduced to a measurement of the orientation, called degree of orientation. Instead of integrating the structure radially, it is integrated in an azimuthal angle, at a constant q-range, as in Figure 3.9.

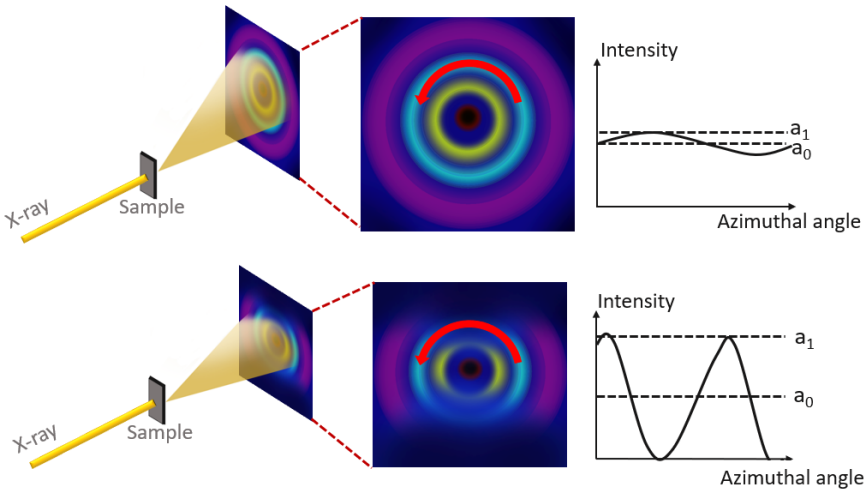

Figure 3.9: The upper figure shows a symmetric scattering which, when integrated in an azimuthal angle, gives small variations in intensity. The lower figure shows an asymmetric scattering pattern which, when integrated in an azimuthal angle, gives large variations in intensity. The value a_1 is the highest value of the intensity while the value a_0 is the average intensity.

In Figure 3.9 the maximum of the intensity is denoted a_1, and called asymmetric intensity, the mean of the intensity is denoted a_0 and is called the symmetric intensity.

The degree of orientation is defined as:

$$\text{Degree of orientation} = \frac{a_1}{a_0} \tag{3.1}$$

For a scanning SAXS or WAXS experiment the degree of orientation can be calculated for every point that has been examined, which makes it possible to distinguish the changes in orientation over the whole scanned sample. The azimuthal integration is not averaged over the whole sample, but only performed in a certain q-range. For the SAXS-experiments the intensity was integrated for a q-value in the range 0.59 nm^{-1} to 1.8 nm^{-1}, which corresponds to the distance d_{ac}. The WAXS results were integrated for q-values in the range of 14 nm^{-1} to 16 nm^{-1}, which corresponds to the orthorombic (110) peak.

4
Results

The characterization of HDPE mainly focused on two different types of samples. The separate layers were analyzed, and the results were used to furthermore discuss the analysis of the full thickness. The separate layers; bulk, and shear, were only investigated when deformed in the CD direction and post-mortem. The samples of the full thickness were deformed in both the MD and the CD directions. The last part of the analysis includes the in-situ measurements of the samples deformed in CD and MD.

The analysis revolves around three concepts; the scattering patterns, the radially integrated data (for an explanation of these, see Section 2.4) and the degree of orientation (see Section 3.4). There were no measurements on completely undeformed HDPE, but the grip is considered the most undeformed part, the neck is more affected and the tip at the rupture is the most deformed part of the dog bones.

4.1 Analysis of the Separate Layers

The bulk and shear samples were produced by grinding samples cut in the CD direction from HDPE plates. The samples were tensile tested until breakage, and the deformed dog bones were measured post-mortem at a synchrotron source.

4.1.1 Analysis of the Bulk Layer

The SAXS and WAXS results of the bulk sample are presented in Figure 4.1.

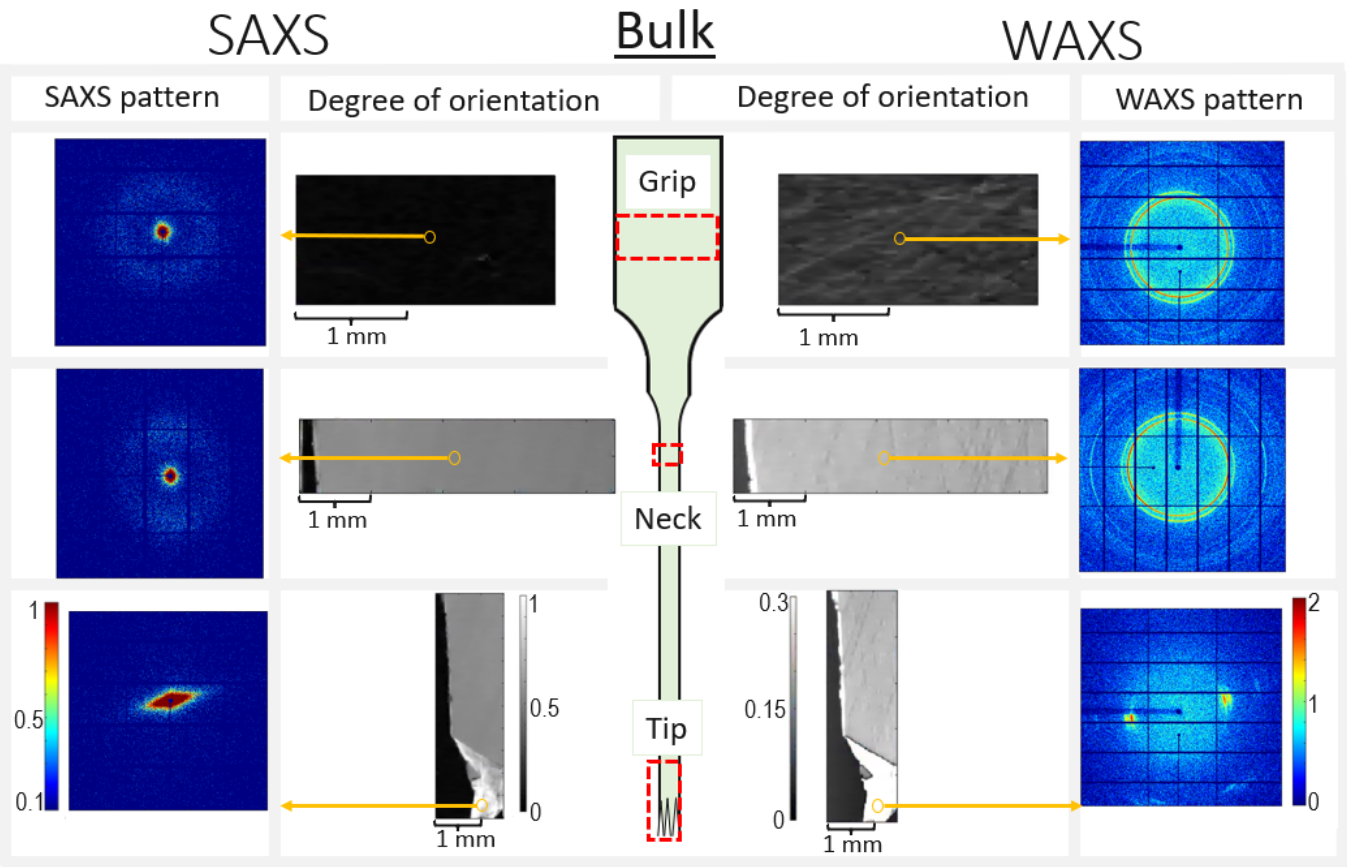

Figure 4.1: The figure shows SAXS and WAXS results of the bulk sample. The grip, the neck, and the tip were investigated separately. The degree of orientation with one corresponding scattering pattern is presented.

In Figure 4.1 only one scattering pattern for each region is shown. The scanning SAXS and WAXS give scattering patterns for points over the whole sample. A selection of these were investigated, however too many to include in this report. The grip and neck have similar scattering patterns over the whole region, thus the scattering patterns shown can be seen as representative of the respective regions. There were different types of scattering patterns in the region of the tip. Most of the tip had the same scattering pattern as the neck, except for the absolute rupture point. The scattering pattern for the tip close to the breaking point is shown in Figure 4.1.

The results of the grip indicate spherical spherulites, due to symmetric structures and a low degree of orientation. The grip region in Figure 4.1 shows a low degree of orientation, which can be seen in the symmetric scattering pattern. The scattering pattern is typical for spherical spherulites. The bulk sample is therefore believed to contain spherical spherulites, which is furthermore supported by literature, as mentioned in the Theory section.

The results of the neck indicate presence of elongated spherulites due to oriented scattering patterns and a higher degree of orientation. Similarly to the discussion of spherical spherulites, the scattering pattern for the neck region

is typical for the elongated spherulites according to literature. This shows that during tensile testing the spherulites are affected by the applied force. The spherulites are elongated in the same direction as the force. The degree of orientation is a measure of the orientation of the sample, and cannot be directly put in relation to a certain type of structure. The degree of orientation is however uniform over the whole necking region, up until the very rupture point of the samples. As mentioned, several scattering patterns were investigated in this region, which were similar to the SAXS scattering patter presented in Figure 4.1. The elongation of the spherulites is assumed to take place when there is necking of the sample, and the spherulites are elongated until very close to the rupture point.

The scattering pattern of the tip indicate that the spherulites have been sheared apart and formed microfibrillar structures. In Figure 4.1 there is a noticeable difference between the SAXS patterns of the neck versus the tip. The tip shows a highly oriented elongated structure instead of the previous circular pattern. When microfibrils are formed there are no longer large lamellae with amorphous regions in between, which means that they no longer can exist in the form of spherulites. This transition can be seen in the SAXS scattering pattern as a highly oriented centered pattern, as can be seen for the tip in Figure 4.1. The WAXS pattern also show a high degree or orientation, which is believed to be caused by the alignment of the polymer chains in the microfibrillar crystalline parts within the sample.

4.1.2 Analysis of the Shear Layer

The results of the deformation of the shear layer are presented in Figure 4.2.

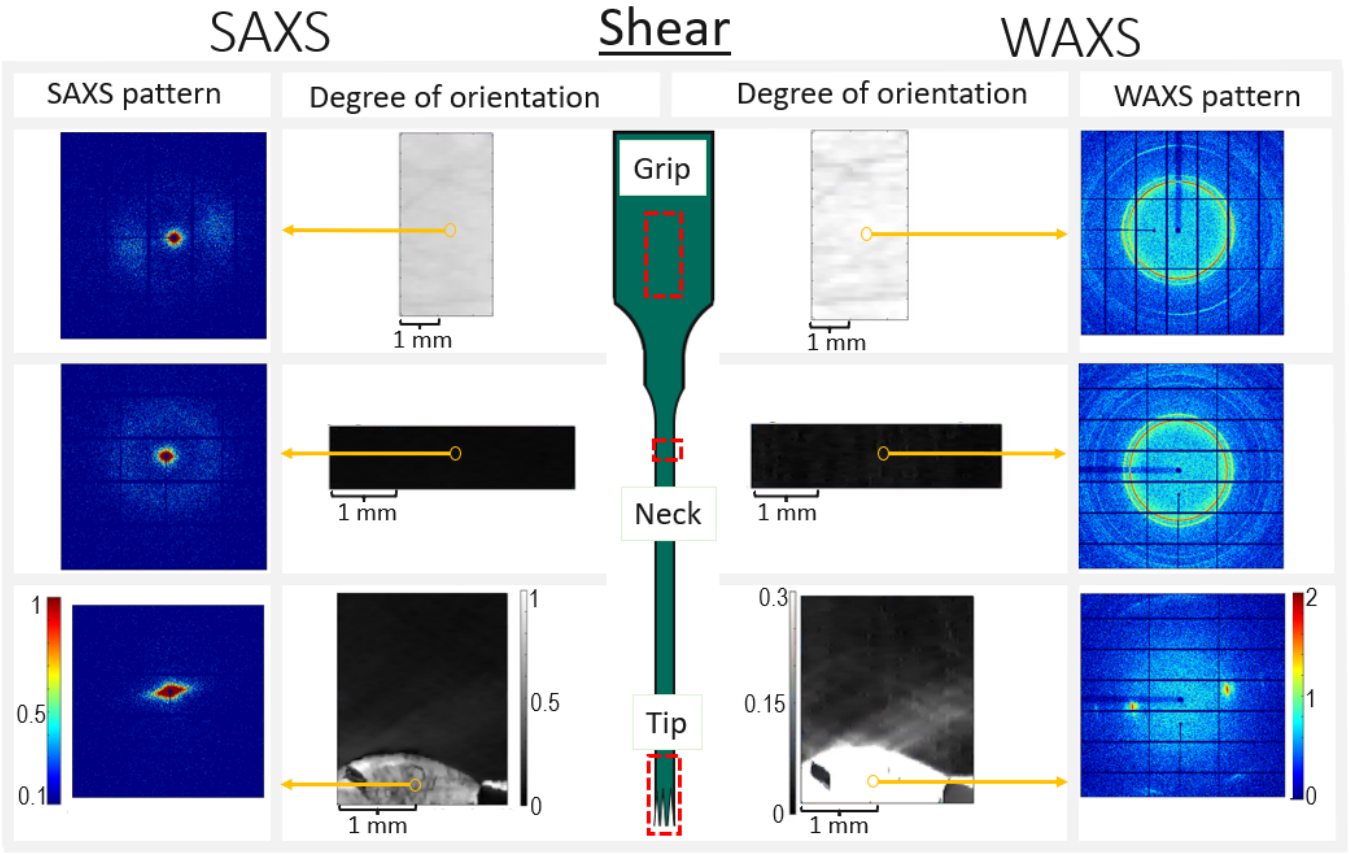

Figure 4.2: The figure shows SAXS and WAXS results of the shear sample. The grip, the neck, and the tip were investigated separately. The degree of orientation with corresponding scattering patterns are presented.

As in the case of the bulk, Figure 4.2 only shows selected patterns for each region. Several more patterns from each region were investigated during the analysis, and the chosen ones can be seen as characteristic for each respective region.

The results of the grip indicate elongated spherulites, due to asymmetric structures and a high degree of orientation. A similar pattern to the elongated spherulites in the bulk can be seen in the region of the grip in Figure 4.2. As mentioned, both the SAXS and the WAXS patterns are typical for elongated spherulites, which is therefore concluded to exist in the shear. The orientation of the elongated spherulites is however in a 90°shift to the bulk-neck patterns. The elongated spherulites in the grip are formed when the polymer crystallizes during the injection molding process, and therefore has the same orientation as the flow. The elongated spherulites that can be seen in Figure 4.2 are therefore formed during manufacturing and are relatively unaffected by the applied force, whereas the elongated spherulites in the bulk samples were the cause of deformation.

The results of the neck indicate existence of spherical spherulites, due to symmetric patterns and a low degree of orientation. In contrast to the bulk, scattering patterns became more symmetric during tensile testing. The scattering

patterns are characteristic for spherical spherulites, so it is assumed that when the elongated spherulites are deformed in the opposite direction of the elongation they will become more spherical, i.e., pulled back into a spherical shape.

The results of the tip indicate that the spherulites have been sheared apart and formed microfibrillar structures. As in the case of the bulk structure the lamellae and the amorphous regions eventually break to become microfibrillar structures. The scattering patterns no longer show trace of spherulites, but instead a very oriented structure structure in both the SAXS and the WAXS results.

4.1.3 Comparison of the Shear and the Bulk Layers

The distance of one crystalline lamella and one amorphous region is denoted d_{ac}. Radial integration of the SAXS data was used to investigate the relationship between the d_{ac} of the spherical and elongated spherulites, in the shear and the bulk samples. When the SAXS data is integrated radially, the highest intensity corresponds to at which q-value the average d_{ac} distance is located. The q-value can be used to calculate the distance d_{ac} according to Equation 2.2. The values of d_{ac} from the shear and bulk layers are presented in Table 4.1.

Table 4.1: Distance of one lamella and one amorphous layer, d_{ac} for the shear and the bulk samples.

Layer	**Sample**	**d_{ac} [nm]**
Bulk	Grip	19.5
	Neck	18.8
	Tip	18.8
Shear	Grip	18.8
	Neck	19.7
	Tip	19.6

The distance of one crystalline lamella and one amorphous region is constant for spherical and elongated spherulites. It can be seen in Table 4.1 that d_{ac} are in a range of 18-20 nm for HDPE, which agrees well to literature values [19]. There are small errors when performing radial integration and fitting of the intensity peak, so these values are considered to be fairly similar. The conclusion is therefore that the the average distance of one lamella and one amorphous region can be assumed to be in the range of 18-20 nm for both the shear and the bulk sample. This means that the shear and bulk contain spherulites of similar structure and that the distance d_{ac} is not affected of the deformation until the spherulites are completely torn apart.

The WAXS patterns were integrated radially to show at which q-values the crystal planes were located. The radially integrated patterns for shear and bulk are pre-

sented in Figure 4.3.

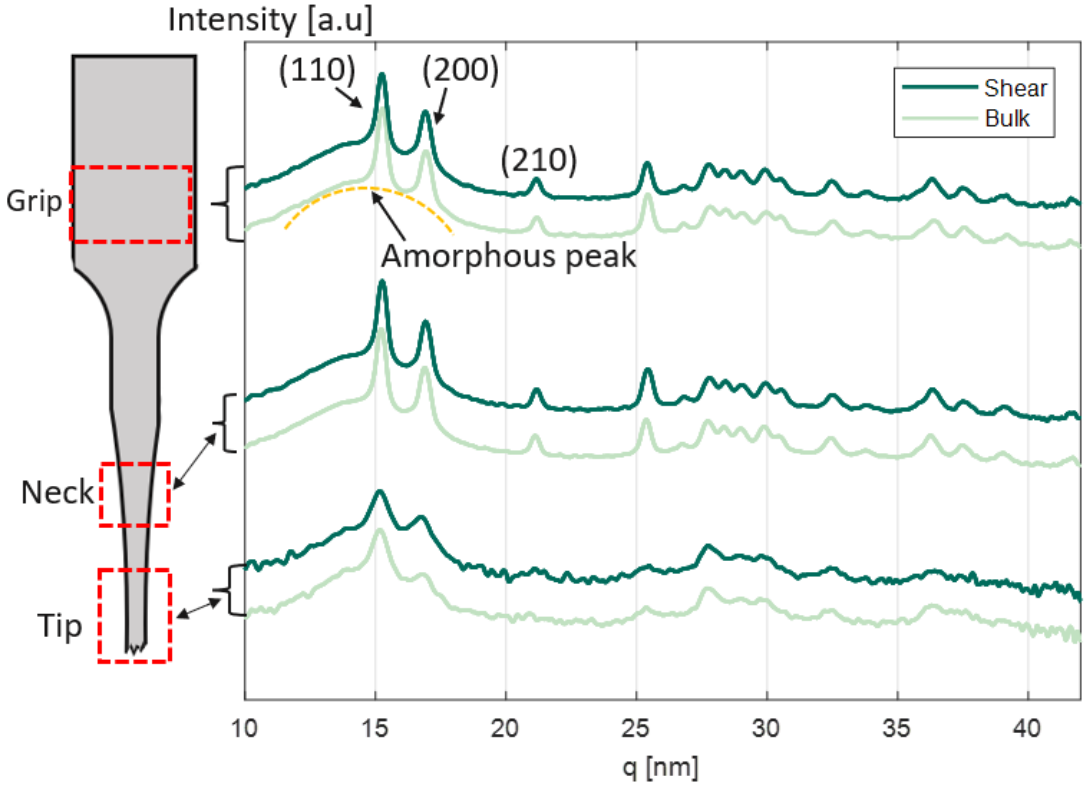

Figure 4.3: Radially integrated intensity plots for the bulk and the shear. All samples are shifted in the y-direction to improve visualization of results. The upper curves represent the grip, the middle curves show the neck and the lower curves represent the tip.

It can be seen in Figure 4.3 that the crystalline unit cells behave similarly for the shear and the bulk. The grip curves look nearly identical and clearly shows the characteristic peaks for HDPE. The peak position for the grip peaks as well as the theoretical values calculated with Equation 2.4 are presented in Table 4.2.

Table 4.2: Theoretical and experimental values of peak positions of the first three peaks of HDPE. The peak positions for the shear and the bulk were identical for the grip and therefore only one values is reported as the experimental value.

	Theoretical		**Experimental**	
Crystal plane	q [nm^{-1}]	d_{hkl} [nm]	q [nm^{-1}]	d_{hkl} [nm]
(110)	15.31	0.41	15.24	0.41
(200)	16.98	0.37	16.91	0.37
(210)	21.20	0.30	21.14	0.30

The crystallinity decreases during deformation. Peaks broaden, decrease and disappear when the material is being deformed. The change of the peaks during deformation indicates that the crystalline lamellae are being deformed. The radially integrated intensity for the tip in Figure 4.3 does not show as clear peaks as for the grip and the neck region. The highest peaks can still be distinguished while the peaks at the lower q-values disappear into the background. During tensile testing several types of deformations take place in the material. Initial deformation includes deformation of the amorphous parts, the random chains become elongated in the direction of the flow of the material. After the deformation of the amorphous parts, the lamellae will be affected. Some polymer chains in the crystalline region will be pulled out of the lamellae into the amorphous phase. As mentioned, amorphous material does not show any long-range orientation, however their short range material orientation can give a broad amorphous peak. Many short-range orientations give rise to the wide peak. The amorphous peak is indicated in Figure 4.3. The crystallinity of the samples can be quantitatively estimated from the ratio of the crystalline to the amorphous peak intensities. It can be seen in Figure 4.3 that the intensity of the crystalline peaks, (110) and (200) decrease while the amorphous peak is increasing. This indicates that the amount of crystallinity in the sample decreases as it is being deformed, due to the fact the chains are drawn out of the crystalline phase into the amorphous parts.

A schematic of the different regions of the shear and bulk samples was produced to visually explain what happens in the material during deformation, see Figure 4.4 and Figure 4.5.

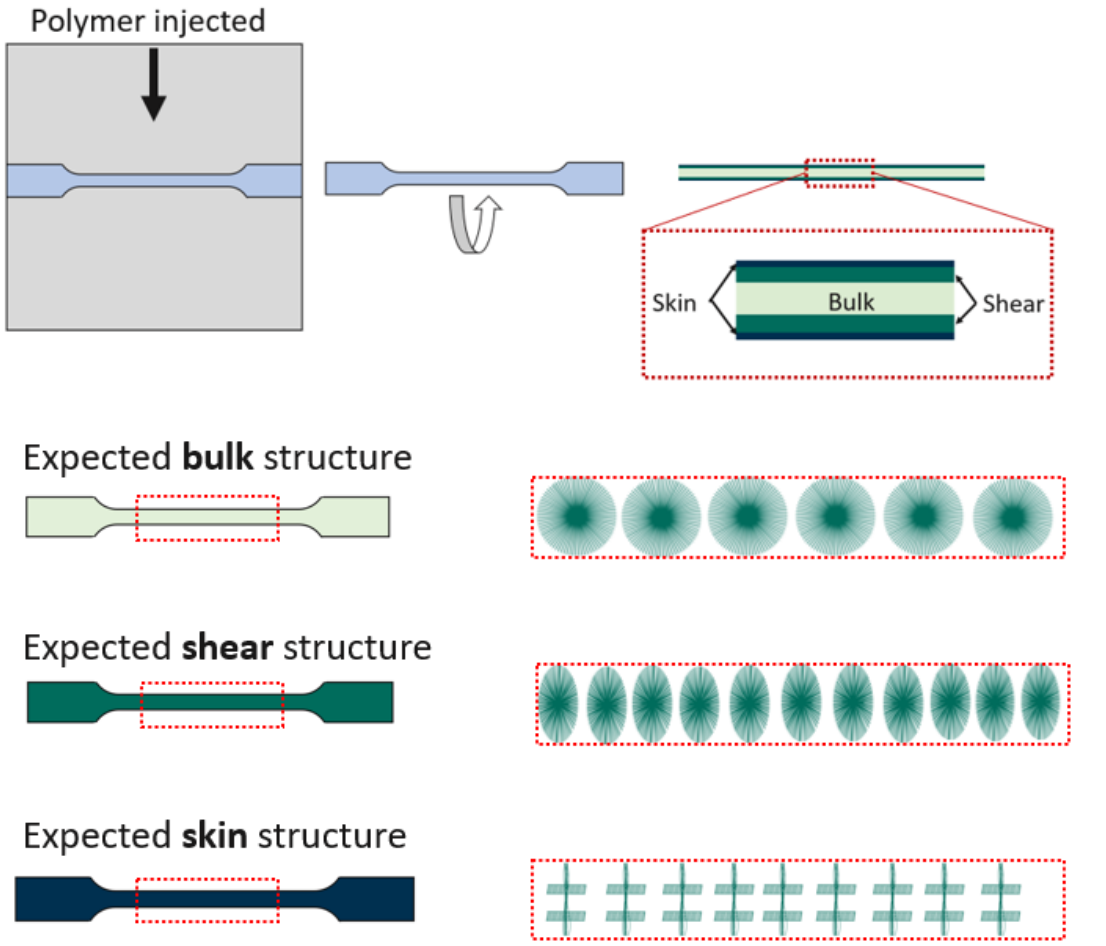

Figure 4.4: The sample was cut from the mold in the CD direction. Through the cross direction of the sample several layers are formed, the skin, shear and bulk layers. These were ground down to separate the layers, and the expected structure of each layer is depicted.

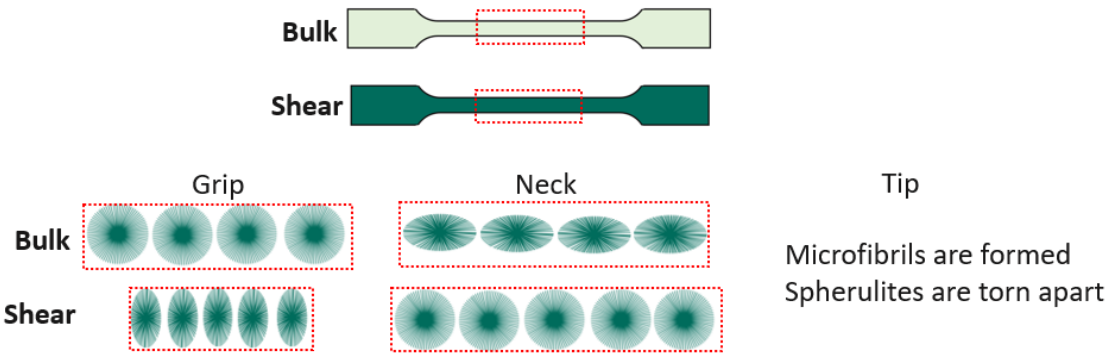

Figure 4.5: The schematic shows how the layers of shear and bulk deforms during tensile testing. The bulk layer contains spherical spherulites which become elongated while the shear contains elongated spherulites which are pulled back into spherical. The spherulites are torn apart at the very tip.

Literature referred to the bulk layer containing spherical spherulites and the shear layer containing elongated spherulites. The spherical spherulites in the bulk layer and the elongation of them can be seen in the SAXS and WAXS results. Furthermore, the opposite behavior that took place in the shear could be observed. In the shear, the spherulites were elongated in yhe grip, to become more spherical in the neck and eventually becoming microfibrillar in the absolute tip. From the conclusions of the shear and the bulk, it can be seen that the two layers have different structures in the grip that behave differently during elongation. Close to the breaking point, the structures in both layers were exposed to a large enough deformation to break the macrostructures of the spherical and elongated spherulites, and the structures became microfibrillar. The results from the bulk and the shear layer will be used when discussing the samples of full thickness.

4.2 Analysis Through Full Thickness in CD and MD

The samples of full thickness contain all layers previously discussed (shear and bulk) as well as the skin layer that contains the shish kebab structure. The samples were deformed in both the MD direction and the CD direction and were analysed post-mortem.

4.2.1 Analysis of the Sample Deformed in the MD Direction

The results from the dog bones deformed in MD, measured by SAXS and WAXS, are presented in Figure 4.6.

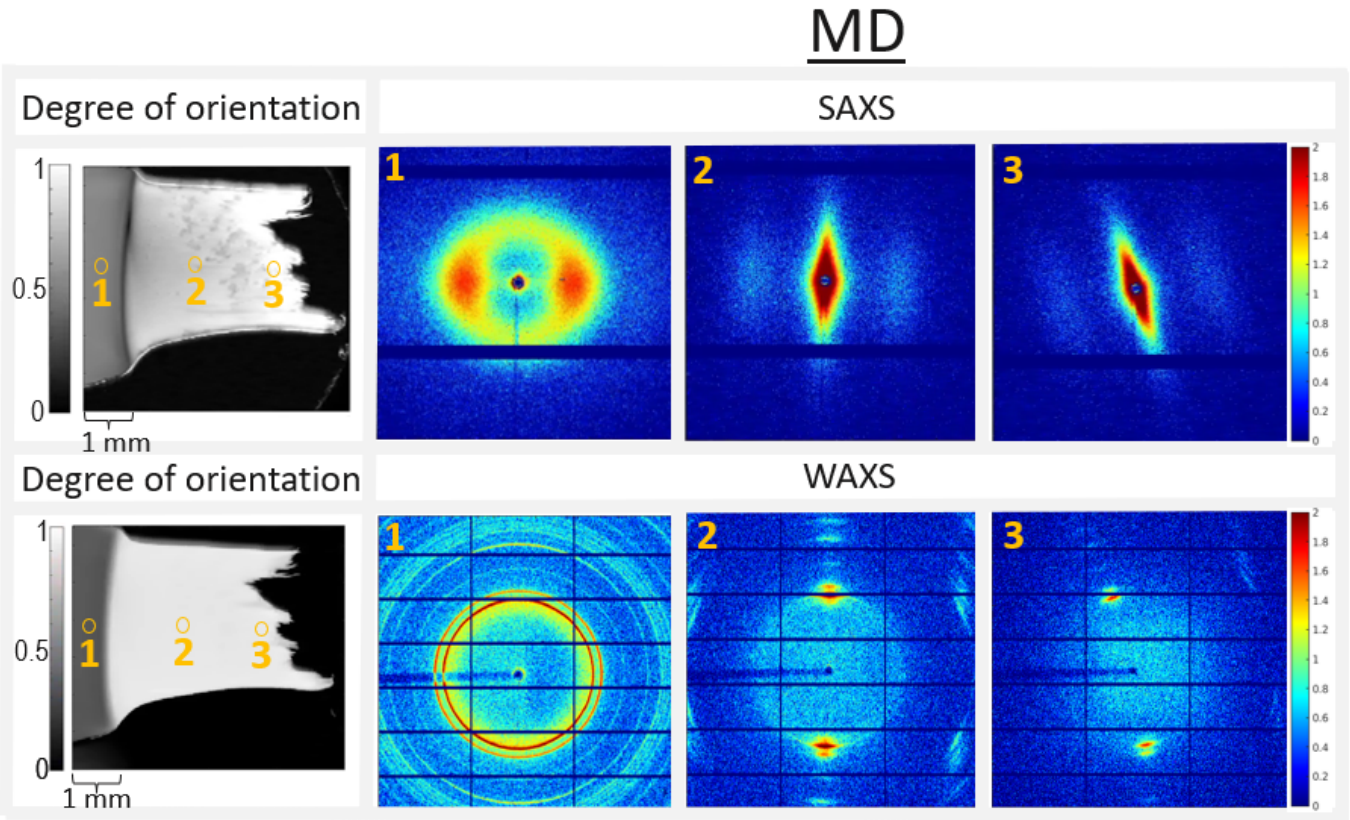

Figure 4.6: The degree of orientation (the left figure) for the whole sample was determined in SAXS (upper row) and WAXS (lower row). In the figure of the degree of orientation three different points, representing 1) Grip, 2) Neck and 3) Tip with corresponding scattering patterns are depicted.

Figure 4.6 shows the scattering patterns for a few points chosen for the sample. Several scattering patterns in each region were investigated, and showed similar structures as reported in the figure. The analysis of the degree of orientation fails for the scattering patterns that no longer show circular patterns. Since the degree of orientation gave a visualization of how the samples looked, the figures are shown. The absolute values of the degree of orientation after the grip region are however not completely reliable. The compilation of results for the MD sample shows several characteristics of the structure of the material.

The grip region exhibits a strong signal from all of the structures. In Figure 4.6, for the SAXS scattering pattern 1, there is a pattern that is very similar to the elongated spherulites (2.23) as well as the results of the elongated spherulites in the shear layer (Figure 4.2). The scattering pattern is more intense than for the sample of only shear. Since the MD sample was measured through all of the layers, the scattering patterns from shish kebab, elongated spherulites and spherical spherulites should be overlaying each other and giving an intense scattering pattern. The layers of full thickness were furthermore thicker than the separate layers, which gives a stronger signal. Scattering from spherical spherulites are hidden by the scattering from the elongated spherulites, and the shish kebab scattering is also hard to

distinguish. The skin layer is the thinnest layer, which might be one of the reasons that the scattering from the shish kebab structures is low in the grip region.

The microfibrils give a strong signal in the neck and at the tip. Shish kebab structures can also be seen. The SAXS patterns 2 and 3 in Figure 4.6 show highly oriented structures in the direction of tensile testing. Similarly to both the SAXS and the WAXS results from the shear and bulk samples, the high orientation means that the sample has become microfibrillar. There are no spherulites left, since the crystalline lamellae have been torn apart to become microfibrils. In contrast to the shear and the bulk sampes, there is some additional scattering from the shish kebab structure, which can be distinguished in the SAXS patterns as additional scattering horizontal to the central scattering slice and in the WAXS patterns as additional scattering clusters. The MD sample contained all the layers, and it is therefore not surprising to see the impact from the shish kebab. Noteworthy, however, is that the shish kebab seems to have an impact on the necking region of the sample. In the shear and the bulk samples, the microfibrils could not be distinguished until the breaking point, while microfibrils can be seen already in the necking region for the sample deformed in MD. The samples deformed in the MD direction could be elongated more than 10 times longer than the bulk and the shear samples. The shish kebab structure therefore has a high impact on the strength of the material. One hypothesis why the microfibrils show already in the neck for the sample deformed in MD is that the spherulites have been torn apart before the shish kebab is affected. The strain needed to deform the spherulites is much smaller than the strain needed to deform the shish kebab structures. The structure has thus become microfibrillar before the shish kebab yields and the material undergoes necking.

4.2.2 Analysis of the Sample Deformed in the CD Direction

The analysis of the results from the dog bone deformed in CD is presented in Figure 4.7.

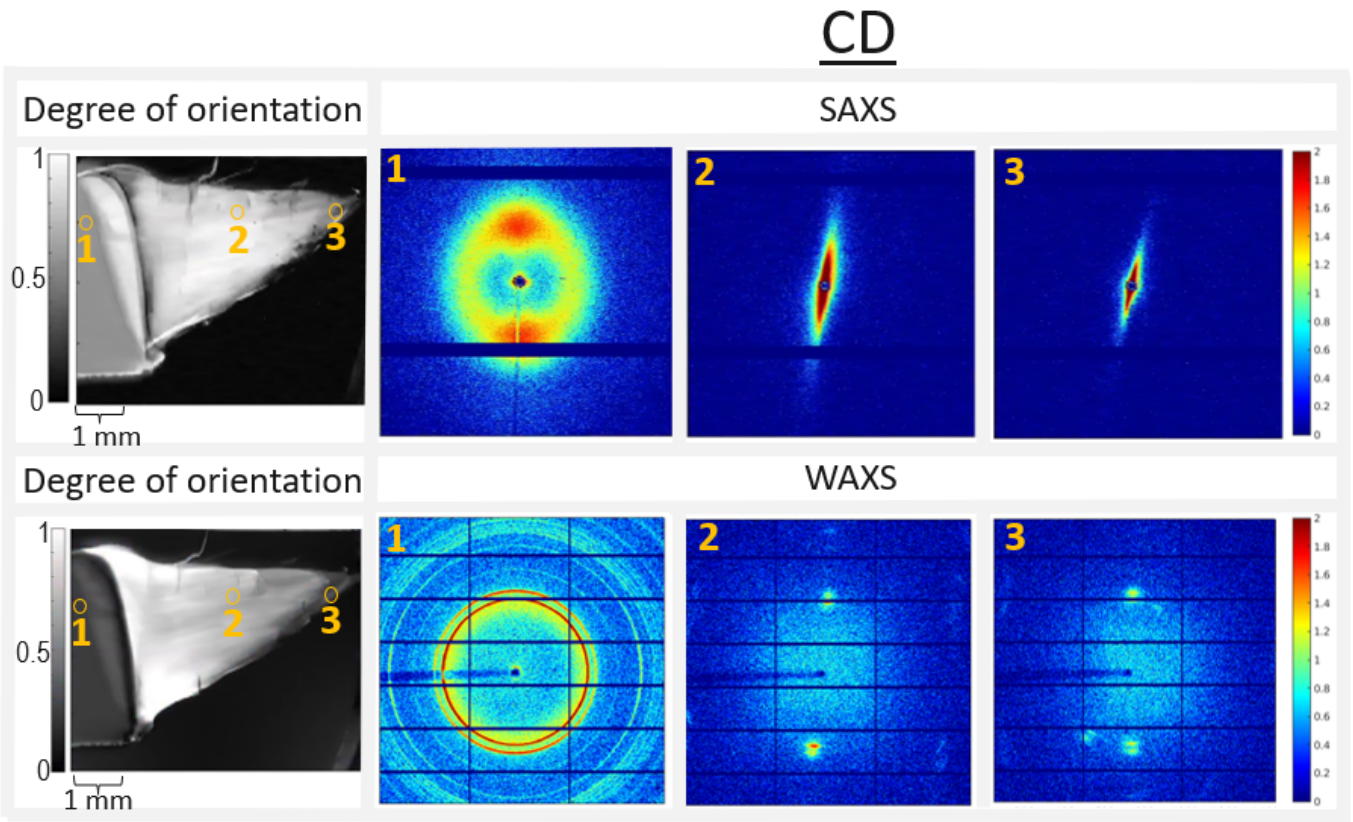

Figure 4.7: The degree of orientation (left) for the whole sample was calculated in SAXS (upper row) and WAXS (lower row). In the figure of the degree of orientation three different points, representing 1) Grip, 2) Neck and 3) Tip with corresponding scattering patterns are depicted.

Figure 4.7 shows representative scattering patters for each region of the sample deformed in CD. As mentioned, the analysis of the degree of orientation fails for microfibrillar samples, but still gives a visualization of how the sample looked. The compilation of results for the sample deformed in CD shows several characteristics of the structure.

The grip region shows a strong signal from all of the structures. The SAXS scattering pattern 1 in Figure 4.7 shows a very similar pattern to MD, but rotated 90 degrees. This was expected since the sample was cut from the HDPE in a 90-degree angle, but mounted for measurements in the same direction as the MD sample. The CD sample of full thickness contains all the layers, and scattering patterns from all structures are therefore expected. The pattern from the elongated spherulites is the most prominent, overlaying the scattering pattern of the spherical spherulites. The shish kebab layer was the thinnest layer is therefore not as easy to detect. The same argument therefore holds for the sample deformed in CD as in MD, that the pattern shows the elongated and spherical spherulites that the HDPE is expected to contain.

The microfibrils give a strong signal in the neck and the tip. Similarly to the MD sample, the spherulitic structures yield long before the shish kebab struc-

ture. In both the neck and the tip region, the microfibrils can be seen in both SAXS and WAXS patterns, due to the highly oriented scattering patterns. In the sample deformed in MD, scattering from the shish kebab structures could be distinguished in both the SAXS and the WAXS patterns, but the same results do not show for the samples deformed in CD. From the scattering results it is not clear what happens with the shish kebab structures. The hypothesis is that when the sample is deformed, the structure is rotated 90°, in the direction of the deformation. No scattering clouds in the horizontal direction of the microfibrillar core in the SAXS pattern can be seen, which might be due to the lamellae in the kebab being completely deformed by the deformation. The hypothesis of the shish kebab deformation is depicted in Figure 4.8.

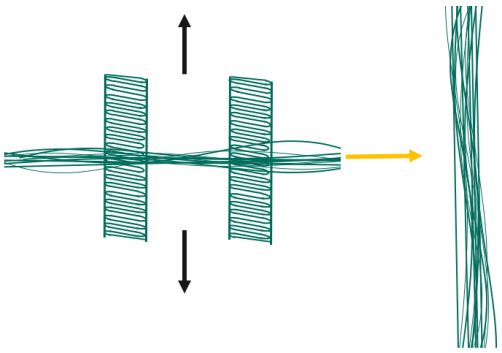

Figure 4.8: Illustration of the hypothesis of the shish kebab deformation. The shish kebab is deformed in the direction of the black arrows. The lamellae might be elongated to fibrils and rotated to be a part of the central fiber core, that is also rotated in the direction of the flow.

4.2.3 Comparison of the Samples Deformed in the MD and CD Directions

The WAXS scattering patterns were integrated radially to create plots that show the distance between the peaks of the patterns. The radially integrated patterns for samples deformed in CD and MD respectively, are presented in Figure 4.9.

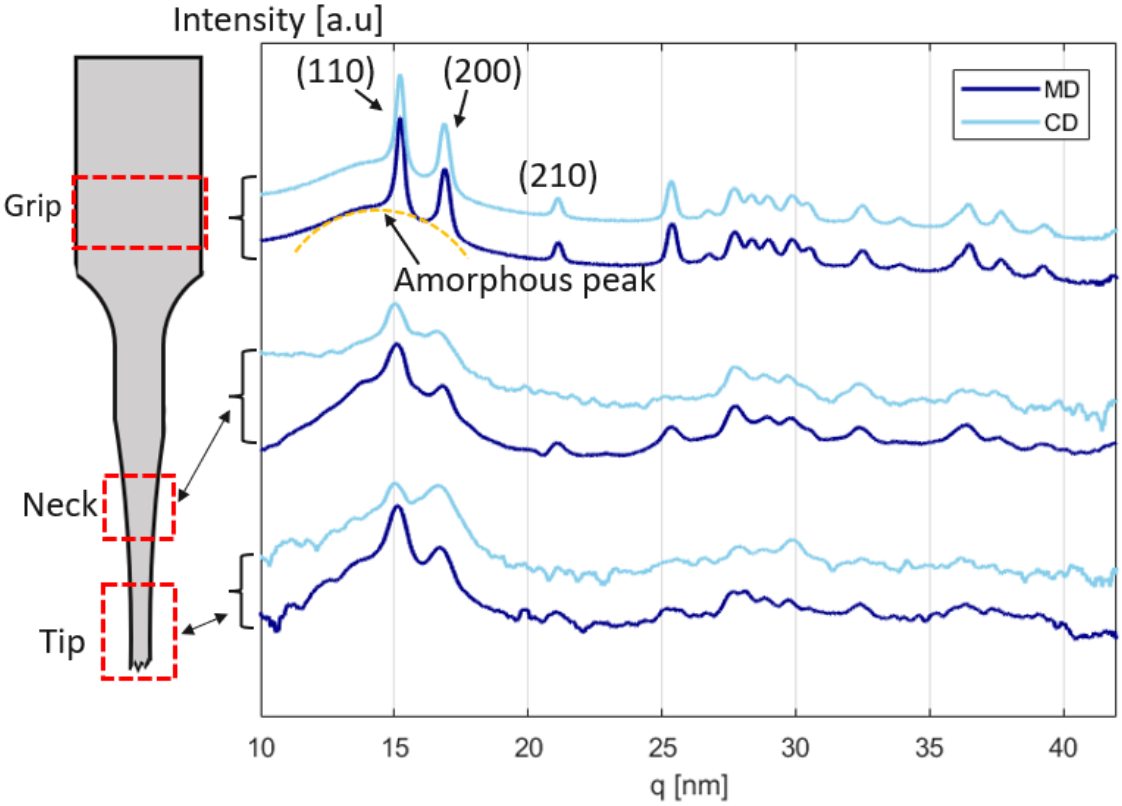

Figure 4.9: Radially integrated intensity plots for MD and CD of full thickness. All samples are shifted in the y-direction to improve visualization of results. The upper curves represent the grip, the middle curves show the neck and the lower curves represent the tip.

The crystallinity decreases during deformation. In Figure 4.9 it can be seen that peaks broaden, decrease and disappear when the material is being deformed. The radially integrated intensity for the neck and the tip in Figure 4.9 does not show as clear peaks as in the grip region. The grip region shows the expected peaks for the crystal planes in HDPE, similarly to the shear and bulk samples. The highest peaks for the neck and the tip can still be distinguished while the peaks for the lower q-values disappear into the background. As in the case of the scattering patterns a big change is seen between the grip region versus the neck and the tip. During tensile testing some of the chains in the lamellae are pulled out to the amorphous regions, leading to a decrease in crystallinity. It can be seen in Figure 4.9 that there is a change between the samples deformed in MD and CD for the neck and the tip. The sample deformed in CD have fewer clear peaks from the (110) and (200) crystal planes and a wider amorphous peak. The shish kebab contains crystalline lamellae, and it could be seen in the samples deformed in CD that the shish kebab might have been deformed significantly, in contrast with the sample deformed in MD. The deformation of the lamellae in the shish kebab might be the reason that the CD show less clear (110) and (200) peaks in the neck and the tip.

A schematic representation of the macrostructures (shish kebab and spherulites) for

the samples deformed in MD and CD was produced to visually explain what happens in the material during deformation, see Figure 4.10.

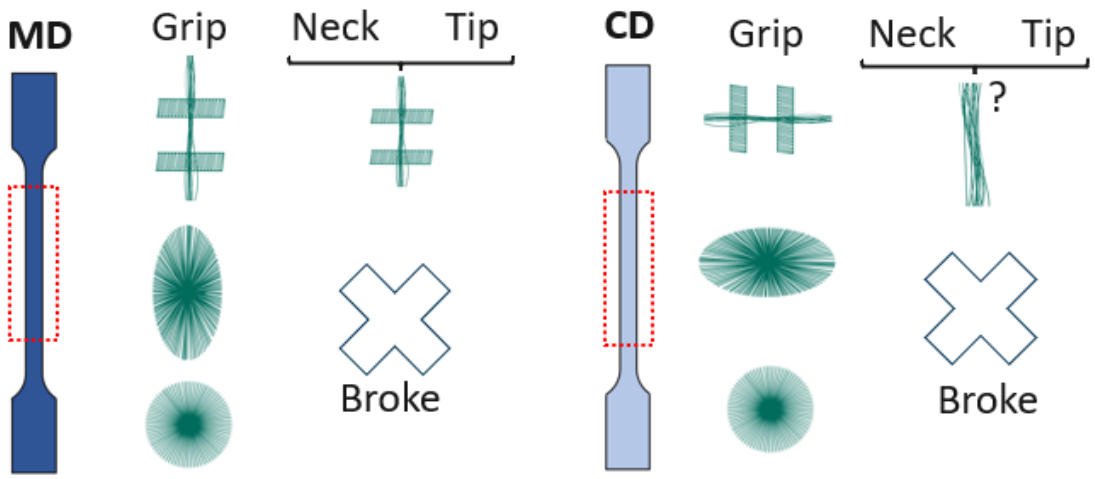

Figure 4.10: The original HDPE plate contain shish kebab, elongated spherulites and spherical spherulites in different layers. The spherulites are torn apart during deformation.

Figure 4.10 illustrate the conclusions from the CD and MD analysis. It can be seen that the grip region consists of all mentioned structures, spherulites and shish kebab. The structures are oriented in a 90° angle to each other since the samples were produced from the HDPE plates in a 90° angle. During tensile testing the spherulite structures are torn apart and become microfibrillar in the neck and the tip. The shish kebab behaves differently between the sample deformed in MD and CD. The MD sample showed scattering from the shish kebab structure, while the CD sample does not. It was hypothesized that the shish kebab deformed in the CD direction is rotated towards the deformation direction and the lamellae being torn info fibers. The complete mechanism of shish kebab deformation is, however, not fully understood.

4.3 In-situ Tensile Tests of Samples Deformed in MD and CD

In the experiments discussed in above sections, dog bones were investigated post-morten, i.e., after deformation and unloading. Dog bones punched in MD and CD respectively, were also investigated by SAXS and WAXS during deformation, i.e., in-situ, to investigate the actual deformation mechanism as well as during unloading. The in-situ experiments were not performed at a synchrotron, and therefore the resolution is worse than measurements reported above. Moreover, the beam did not scan the whole sample, instead only one point of the sample was measured. The

tensile stage used, was not long enough to stretch the samples until breakage. The sample was placed in the tensile stage and pulled simultaneously as several scattering experiments took place. Scattering patterns were collected in 10-second intervals, which corresponds to one measurement. The time evolution of the experiments was called the measurement number, and denoted how many 10-second interval measurements that had taken place.

4.3.1 Analysis of the In-Situ Tensile Testing of Sample Deformed in the MD Direction

The SAXS results for in-situ deformation in the MD direction are presented in Figure 4.11.

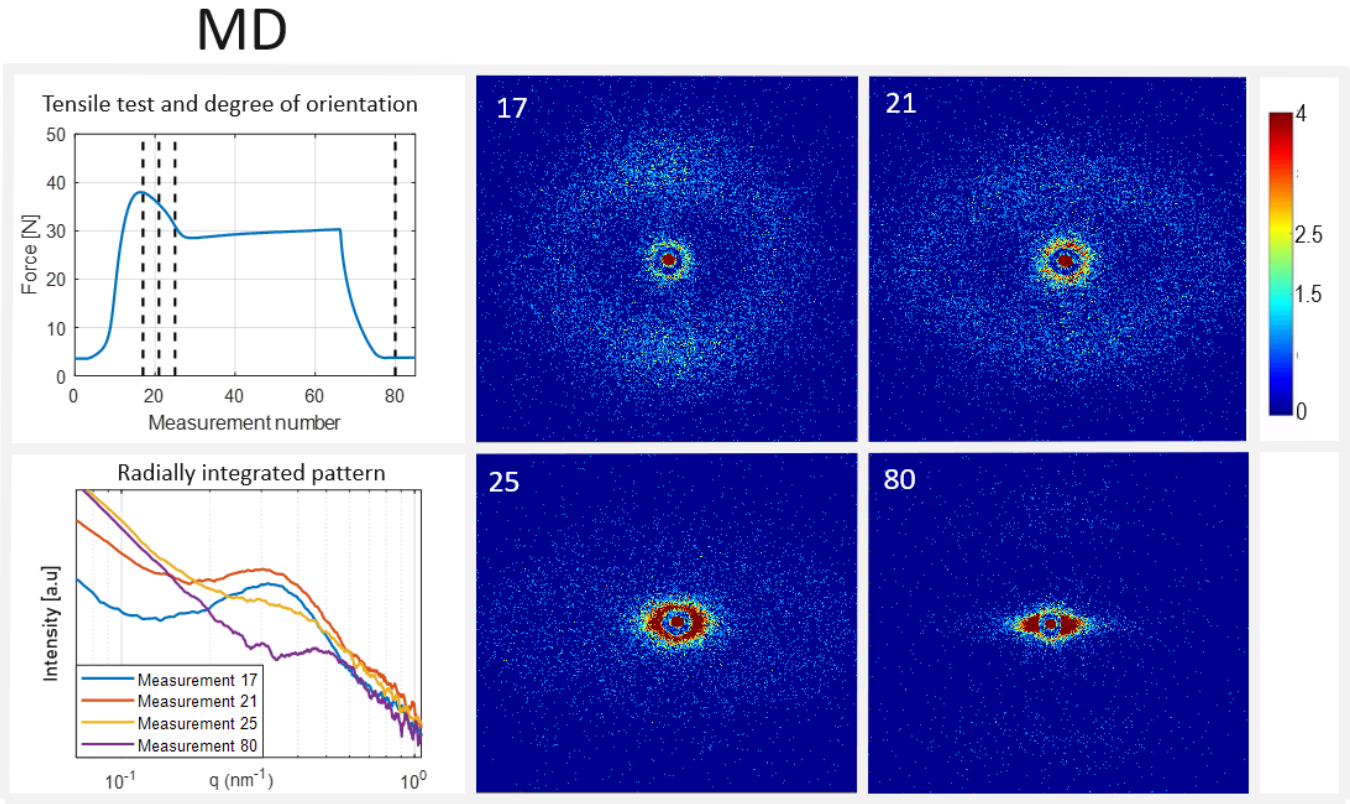

Figure 4.11: The upper left figure shows the tensile curve. The four scattering patterns that are seen to the right are marked with black dotted lines. The lower left figure shows the radially integrated pattern for the chosen scans.

The tensile data in Figure 4.11 shows the typical tensile curve of a polymer, as shown in Figure 2.18. The first yield point is located at measurement 17, and the second yield point is located in between measurement 21 and 25. The scattering pattern changes from a circular pattern up to measurement 17, and then becomes intense and oriented after measurement 25. The scattering patterns in Figure 4.11 were chosen to represent the transition of the scattering. It can, for example, be seen that the patterns do not change significantly between measurement 32 and 80.

It is noteworthy that the tensile stage could not deform the samples until rupture. The deformation range was not big enough to make the elastic HDPE samples break.

The material became microfibrillar after the second yield point. The initial scattering pattern, for measurement 17, is similar to the grip region of the MD sample, and is considered to be the scattering pattern of the almost undeformed sample. Up until the 17th measurement, at the first yield point, the sample is elastically deformed and could regain the original shape if the stress was decreased. Between the 17th measurement and the 25th measurement, there was a significant change of the scattering pattern, from being circular to highly oriented. The scattering pattern from measurement 25 and onwards is similar to the microfibrillar scattering patterns seen in the measurement of the sample of MD measured post-mortem. The in-situ measurement could monitor the transition between elongated spherulites in the elastic region to microfibrillar structures in the plastic region. It can be seen that the transition to microfibrils occurred after the second yield point, which is where the material structures are irreversibly changed. Thus, the transition from spherulites to microfibrils could be followed and occurred after the second yield point.

The WAXS scattering patterns of the sample deformed in MD is presented in Figure 4.12 and the tensile measurement as well as the radially integrated patterns are presented in Figure 4.13.

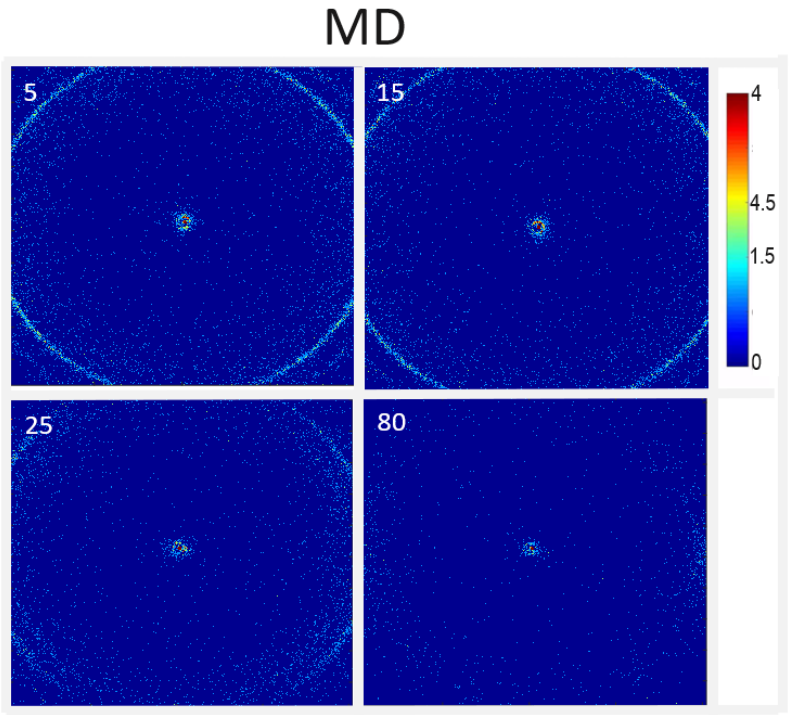

Figure 4.12: The scattering patterns of several in-situ measurements of samples deformed in MD are presented. Scattering pattern 5 represents the undeformed sample, scattering pattern 15 shows the scattering in the elastic region during deformation, scattering pattern 25 shows the scattering around the 2nd yield point and scattering pattern 80 shows the scattering of the sample after deformation.

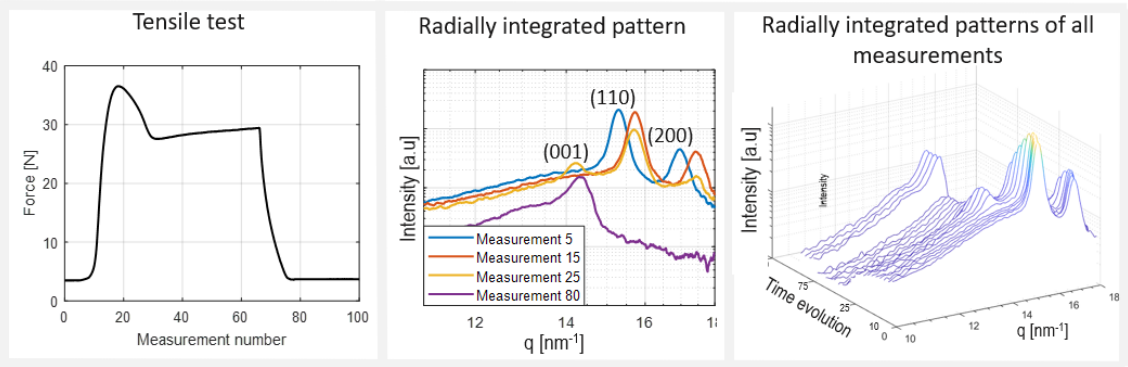

Figure 4.13: The results from the tensile test is presented in the left figure. The middle graph shows the radially integrated curves of a few chosen measurements from the different regions in the tensile curve. The radially integrated pattern to the right is represented in a three-dimensional plot, where all the radially integrated patterns are ordered after each other.

Figure 4.12 shows the WAXS patterns for three chosen measurements, with very weak intensities compared to the synchrotron measurements. The peaks from the (110), (200) and the amorphous peaks could, as expected, be distinguished, but no crystal planes with larger indices. The resolution was expected to be lower for these experiments, due to the measurements being performed in a lab and not at a synchrotron source. The sample could not be placed closer to the detector, due to the large tensile stage. A portion of the scattering pattern thus ended up outside of the detector. It can be seen in scattering pattern 1 in Figure 4.12, even when there was a clear peak, the complete circle could not be detected with the lab equipment. It is important to keep in mind when discussing the data, that parts of the scattering patterns are undetected.

The martensitic transition can be observed. HDPE is known to show a martensitic transition while being subject to a force. This feature is only possible to measure in-situ, since the material transitions back to its original unit cell when the stress is released. From the WAXS investigation of the MD sample, the martensitic transition could be detected. When the material undergoes the martensitic transition the unit cell changes from the orthorombic unit cell to the monoclinic unit cell, which leads to a change in the scattering pattern. A trait of this transition is a decrease of the (110) peak of the orthorombic unit cell with a simultaneous rise of the (001) peak of the monoclinic unit cell [20]. The martensitic transition could not be followed throughout the whole experiment, since the structures became oriented during tensile testing. When the patterns became oriented, they could no longer be monitored with the detector since the orientation made the scattering appear outside of the range of the detector. The orientation of the pattern indicates that the sample has become highly oriented, which could be caused by the sample becoming microfibrillar. During tensile testing the force was eventually released and peaks with higher intensities could once more be distinguished the radially integrated pattern. This should indicate of the reappearance of the ortorombic structure, but since the structure had become much more oriented the scattering could barely be

detected. The martensitic transition could therefore be detected with the in-situ measurements, but not completely monitored throughout the whole experiment.

4.3.2 Analysis of the In-Situ Tensile Testing of Sample Deformed in the CD Direction

The SAXS measurements of the sample deformed in CD are presented in Figure 4.14.

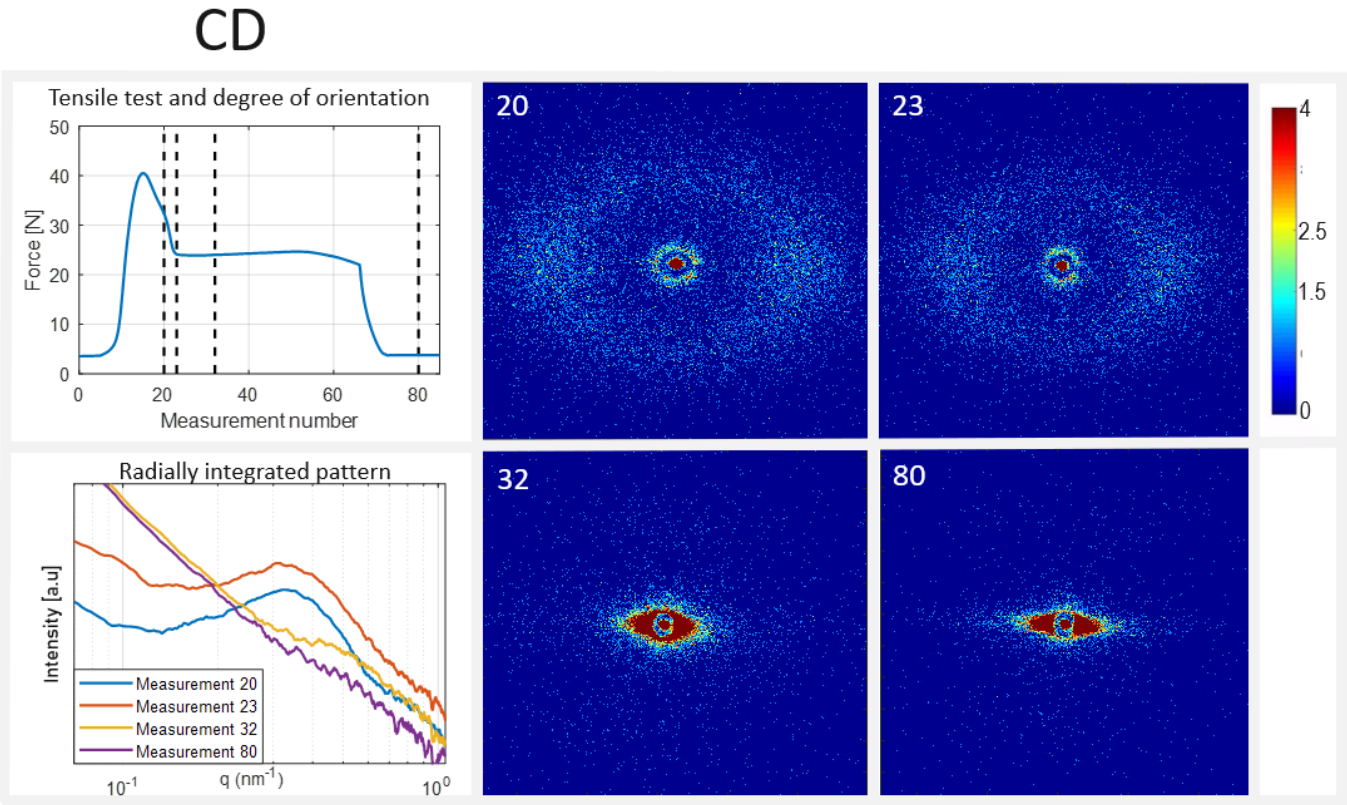

Figure 4.14: The upper left figure shows the tensile curve. The four scattering patterns that are seen to the right are marked with black dotted lines. The lower left figure shows the radially integrated pattern for the chosen scans.

The tensile data in Figure 4.14 show the typical tensile curve of a polymer. The first yield point is located around measurement 17 and the second yield point around measurement 21. The scattering pattern changes from a circular pattern to a highly oriented one between measurement 23 and 32. The pattern then does not change during the rest of the experiments, which can be seen through the similarity of measurement 32 and 80. The deformation range was not big enough to make the elastic HDPE samples break, only elongate.

The material became microfibrillar after the second yield point. The scattering patterns between measurement 1 and 20 look similar and show elongated

spherulites. There is probably scattering from spherical spherulites and the shish kebab layer as well, but as discussed for the post-mortem measurements of the samples of full thickness, these patterns are not as prominent as the elongated spherulites. Between measurement 20 and 32 the scattering pattern changes to indicate the formation of microfibrils. As in the case of the sample deformed in MD, the in-situ measurements could monitor the transition between spherulites to microfibrils. It can be seen that the transition to microfibrils occurred after the second yield point, and the structures are irreversibly changed. Worth noting is that the structural transitions did not seem to coincide with the yield points from the tensile data. In the case of the MD sample the microfibrils could be related to the second yield point, a conclusion that is not clear in the case of the sample deformed in the CD direction. The experimental setup could be a reason of this. The intent was to focus the beam at the thinnest part of the dog bone, and that the necking should occur at that point. There might be an offset of the beam and the first necking point. The consequence of this offset would be that the scattering patterns were not measured at the first formation of the necking, and therefore the microfibrillar transition is not connected to the yield points. To investigate if the offset was due to experimental causes, or a property of the material deformed in CD several samples should be measured.

The WAXS scattering patterns of of the CD sample is presented in Figure 4.15 and the tensile measurement as well as the radially integrated patterns are presented in Figure 4.16.

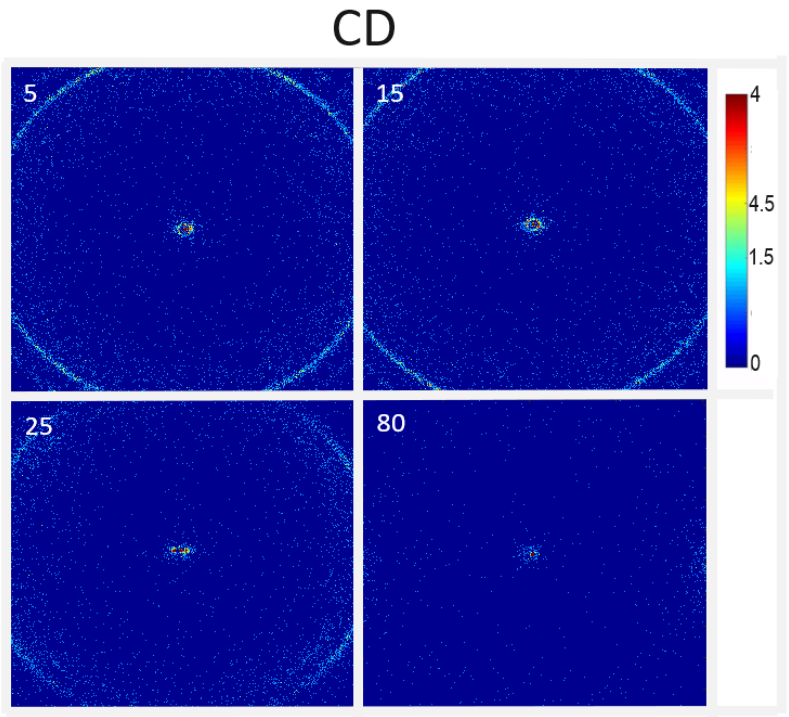

Figure 4.15: The scattering patterns of several in-situ measurements of samples deformed in CD are presented. Scattering pattern 5 represents the undeformed sample, scattering pattern 15 shows the scattering in the elastic region during deformation, scattering pattern 25 shows the scattering around the 2nd yield point and scattering pattern 80 shows the scattering of the sample after deformation.

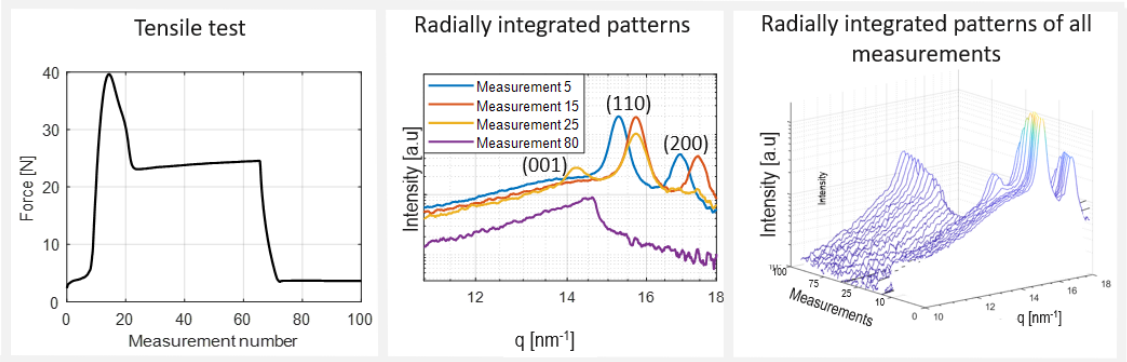

Figure 4.16: The results from the tensile test is presented in the left figure. The middle graph shows the radially integrated curves of a few chosen measurements from the different regions in the tensile curve. The radially integrated pattern to the right is represented in a three-dimensional plot, where all the radially integrated patterns are ordered after each other.

As in the case of the MD sample, only the first peaks, (110), (200), and the amorphous peak could be detected with the WAXS experiment due to the sample not being close enough to the detector. Similarly to the MD sample one interesting feature of the WAXS analysis could be seen.

The martensitic transition can be observed. Equivalently to the sample deformed in MD, the martensitic transition could be detected during WAXS experiments. The transition took place through a decrease of the (110) peak of the orthorombic unit cell with an appearance of the (001) peak of the monoclinic one, as shown in Figure 4.16. Once again, the complete process could not be monitored since the scattering pattern became more oriented and could no longer be detected.

4.3.3 Comparison of the In-Situ Tensile Tests of the Samples Deformed in the MD and CD Directions

To sum up the in-situ experiments, a description of how the deformation of the structures within the material deformed could be obtained. The samples could not be deformed until rupture, but the results of the neck coincide with the results from the samples measured post-mortem. The similarity between the end product of the in-situ measurements and the post-mortem samples shows that once the material was deformed, after the second yield point, the deformation of the structures in the material are irreversible. The samples are therefore permanently deformed. The martensitic transition could be observed for both samples. Since the MD and CD sample contain identical lamellae, with identical crystal structure, the martensitic was expected to appear in both samples.

The most notable difference between the samples is that the MD sample show structural changes connected to the yield points, while the CD sample show no connection. The MD sample became microfibrillar linked to the second yield point, while the CD sample transformed after the neck stabilization point. If this is an issue of the experimental setup or an inherent property of the material, is not possible to deduce from the results presented. More experiments are needed to explain the phenomenon. The tensile curves differ for the MD and CD samples. The first yield point of the MD sample occurred after an elongation of 1.7 mm, while the CD sample only was elongated 1.3 mm before the first yield point was reached. The second yield point and the neck stabilization were also reached for at shorter elongation in the CD direction than in the MD direction. For future work it would be of interest to connect the structures in the material to the differences in the tensile curves.

5
Conclusion

The aim of this project was to contribute to the knowledge of the HPDE structure, more precisely, to investigate the structural change during mechanical deformation of the material. The investigation utilized both synchrotron X-ray sources after deformation, as well as laboratory X-ray sources during deformation. The material was manufactured through injection molding, which made the material anisotropic. To analyze the different structures that are formed during production, the material was cut in two different ways, CD, and MD. The material was furthermore separated into the layers that the material consists of, and the layers; shear, and bulk, were investigated separately.

The methods for characterization were SAXS and WAXS. Using previously known scattering patterns of structures, radially integrated data, as well as the degree of orientation the HDPE structures could be identified. SAXS and WAXS showed to be powerful tools of investigation, the experiments were non-destructive, quick and gave much information about the structures.

The separate bulk and shear layers were first investigated. The SAXS experiment showed how the symmetric spherulites of the bulk were deformed to become more elongated, while the elongated spherulites in the shear layer were pulled back into a spherical structure. At the very breaking point of the material, the structures had become microfibrillar. In-situ tensile tests of the shear and bulk layers would contribute to the understanding of the structural changes during tensile tests.

The full samples, containing all the layers, cut out in the CD and MD direction exhibited the expected structures; spherulites, and shish kebab. The SAXS measurement showed that during deformation the spherulites were torn apart to create microfibrillar structures. The microfibrils appeared already in the necking region, showing the impact of the shish kebab layer. The shish kebab layer could be seen in the measurements of the MD sample, but it was more complicated to explain the shish kebab deformation in the CD samples. The shish kebab layers might have been rotated in the direction of the flow. The WAXS experiments showed that the ordered crystal planes were torn apart during deformation and that the amorphous quantity of the material increased while the crystallinity decreased.

The in-situ tensile tests showed microfibrillation after the second yield point. The samples deformed in the MD direction showed a connection between formation of microfibrils and the second yield point. The same result could not be seen in the

sample deformed in the CD direction. Furthermore, it was shown that HDPE goes through a martensitic transition during tensile testing.

5.1 Further Investigations

In this work, the structural changes of HDPE were investigated during deformation. A selection of samples was chosen for these experiments. The results in this work indicate that there is anisotropy of structures over the plate. To gain understanding in the anisotropy more of the HDPE plates should be investigated. Further work could therefore also include investigations of more dog bones, as depicted in Figure 5.1.

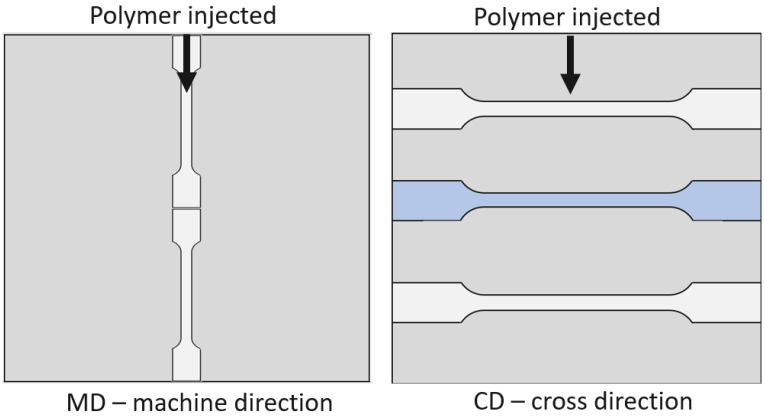

Figure 5.1: Smaller dog bones could be used for further investigations in the MD direction, as presented to the right. Dog bones from the CD direction cut from different positions on the plate are marked in white. Dog bone, in the CD direction, investigated in this work is marked with blue.

Figure 5.1 shows how to place the dog bones to enhance the understanding of the anisotropy. The current size of the dog bones covers the whole MD direction, but to investigate the differences in the direction of the flow, smaller dog bones should be used. More than one sample could thus fit on the plate and be compared to the others. In the CD direction it is possible to obtain dog bones from positions further up and below the current position of the cross direction, which could be analysed and compared to one another. To get a comprehensive understanding of the structures it would also be of interest to connect the structures of the material to the different tensile curves of the samples deformed in MD and in CD.

The in-situ tensile tests of CD and MD could show the process of deformation and gave information of structural changes at the first and second yield point of the material. The shear and bulk samples were too thin to be used by the current tensile stage, but with different laboratory equipment it could be of interest to also include shear and bulk in the in-situ analysis. The deformation of the spherulites could then be monitored more closely without the shish kebab structures contributing to the

scattering. For future work it would furthermore be of interest to isolate and analyse the shish kebab layer. To obtain the thin skin layers, the method for grinding samples must be developed.

To obtain more precise results the in-situ experiments could be performed at synchrotron sources to dramatically increase the resolution of the data.

Bibliography

[1] C. Sagan, L. Margulis, and D. Sagan, "Life - Production of polymers | Britannica," 2022, obtained 2022-03-07. [Online]. Available: https://www.britannica.com/science/life/Production-of-polymers

[2] J. Cowie and V. Arrighi, *Polymers: Chemistry and physics of modern materials*, 3rd ed. Taylor and Francis group, 2007.

[3] J. P. Greene, *Sustainable plastics : environmental assessments of biobased, biodegradable, and recycled plastics*, 1st ed. New Jersey: John Wiley & Sons, Inc, 2014.

[4] Tetra Pak, "Tetra Pak history | Tetra Pak." [Online]. Available: https://www.tetrapak.com/about-tetra-pak/the-company/history

[5] H. Ljungkvist Nordin, A.-K. Westöö, and L. Sörme, "Plastic in Sweden Facts and Practical Advice," Naturvårdsverket, Tech. Rep., 2019.

[6] X. Zhao, K. Cornish, and Y. Vodovotz, "Narrowing the Gap for Bioplastic Use in Food Packaging: An Update," *Environmental science & technology*, vol. 54, no. 8, pp. 4712–4732, 2020.

[7] L. Lin and A. S. Argon, "Structure and plastic deformation of polyethylene," *Journal of Materials Science 1994 29:2*, vol. 29, no. 2, pp. 294–323, 1994.

[8] E. J. Mittemeijer, *Fundamentals of materials science: The microstructure-property relationship using metals as model systems*. Springer Berlin Heidelberg, 2011.

[9] W. Massa, *Crystal Structure Determination*, 5th ed. Springer Berlin Heidelberg, 2004.

[10] T. L. Alford, L. C. Feldman, and J. W. Mayer, "Fundamentals of nanoscale film analysis," *Fundamentals of Nanoscale Film Analysis*, pp. 1–338, 2007.

[11] P. Willmott, *An introduction to synchrotron radiation*, 2nd ed. Hoboken, New Jersey: John Wiley & Sons, Ltd, 2019.

[12] B. Chaudhuri, I. G. Muñoz, S. Qian, and V. S. Urban, *Biological Small Angle Scattering: Techniques, Strategies and Tips*, ser. Advances in Experimental Medicine and Biology. Singapore: Springer Singapore, 2017.

[13] J. Cowie and V. Arrighi, *Polymers: Chemistry and Physics of Modern Materials*, 3rd ed. Boa Raton: CRC press, 2007.

[14] D. P. Malpass, *Introduction to industrial polyethylene.* Salem, Massachusettes: John Wiley & Sons, Ltd, 2010.

[15] S. S. Katti and M. Schultz, "The microstructure of injection-molded semicrystalline polymers: A review," *Polymer Engineering & Science*, vol. 22, no. 16, pp. 1001–1017, 1982.

[16] P. Fratzl and R. Weinkamer, "Nature's hierarchical materials," *Progress in Materials Science*, vol. 52, no. 8, pp. 1263–1334, 2007.

[17] B. A. Schrauwen, *Deformation and failure of semi-crystalline polymer systems*, 1st ed. Eindhoven, The Netherlands: University press facilities, 2003.

[18] E. Piorkowska and G. C. Rutledge, *Handbook of polymer crystallization.* New Jersey: John Wiley & Sons, Inc, 2013.

[19] M. F. Butler, A. M. Donald, W. Bras, G. R. Mant, G. E. Derbyshire, and A. J. Ryan, "A Real-Time Simultaneous Small- and Wide-Angle X-ray scattering study of In-Situ Deformation of Isotropic Polyethylene," *Polymers*, vol. 28, no. 19, pp. 6383–6393, 1995.

[20] L. Wang, J.-H. Wang, B. Yang, Y. Wang, Q.-P. Zhang, M.-B. Yang, and J.-M. Feng, "A novel hierarchical crystalline structure of injection-molded bars of linear polymer: Co-existence of bending and normal shish-kebab structure," *Colloid and Polymer Science*, vol. 291, 2013.

[21] O. O. Mykhaylyk, P. Chambon, C. Impradice, J. P. A. Fairclough, N. J. Terrill, and A. J. Ryan, "Control of structural morphology in shear-induced crystallization of polymers," *Macromolecules*, vol. 43, no. 5, pp. 2389–2405, 2010.

[22] A. Pawlak, A. Galeski, and A. Rozanski, "Cavitation during deformation of semicrystalline polymers," *Progress in Polymer Science*, vol. 39, no. 5, pp. 921–958, 2014.

[23] Z. Bartczak and A. Vozniak, "WAXS/SAXS study of plastic deformation instabilities and lamellae fragmentation in polyethylene," *Polymer*, vol. 177, pp. 160–177, 2019.

[24] T. Seto, T. Hara, and K. Tanaka, "Phase Transformatin and Deformation Processes in Oriented Polyethylene," *Japanese Journal of Applied Physics*, vol. 7, no. 1, 1968.

[25] N. W. Brooks, A. P. Unwin, R. A. Duckett, and I. M. Ward, "Double Yield Points in Polyethylene: Structural Changes Under Tensile Deformation," *Journal of Macromolecular Science, Part B*, vol. 34, no. 1-2, pp. 29–54, 1995.

[26] M. F. Butler, A. M. Donald, and A. J. Ryan, "Time resolved simultaneous small- and wide-angle X-ray scattering during polyethylene deformation - II. Cold drawing of linear polyethylene," *Polymer*, vol. 39, no. 1, pp. 39–52, 1998.

[27] D. Mi, M. Zhou, and J. Zhang, "Quantification of shish–kebab and β-crystal on the mechanical properties of polypropylene," *Journal of Applied Polymer Science*, vol. 134, no. 28, 2017.

DEPARTMENT OF PHYSICS
CHALMERS UNIVERSITY OF TECHNOLOGY
Gothenburg, Sweden
www.chalmers.se

CHALMERS
UNIVERSITY OF TECHNOLOGY